Shear-induced phase transitions in fluids confined between chemically decorated substrates

2000 J. Phys.: Condens. Matter 12 1569

(http://iopscience.iop.org/0953-8984/12/8/302)

J. Phys.: Condens. Matter **12** (2000) 1569–1594. Printed in the UK PII: S0953-8984(00)10042-6

Shear-induced phase transitions in fluids confined between chemically decorated substrates

Henry Bock and Martin Schoen†

Institut für Theoretische Physik, Technische Universität Berlin, Hardenbergstraße 36, D-10623 Berlin, Germany

E-mail: henry@ozon.physik.tu-berlin.de and m.schoen@physik.tu-berlin.de

Received 2 December 1999

Abstract. In this paper we investigate the phase behaviour of a 'simple' fluid confined to a slit of nanoscopic width s_z by chemically decorated, plane-parallel substrates consisting of slabs of weakly and strongly adsorbing solid which alternate in the x-direction with period s_x. In the y-direction the substrates, occupying the half-spaces $-\infty \leqslant z \leqslant -s_z/2$ and $s_z/2 \leqslant z \leqslant \infty$, are translationally invariant. On account of the interplay between confinement (i.e., s_z) and chemical decoration, three fluid phases are thermodynamically permissible, namely (inhomogeneous) gaslike and liquidlike phases and 'bridge phases' consisting of high(er)-density fluid over the 'strong' part which alternates in the x-direction with low(er)-density fluid over the 'weak' part of the substrate. In the x–y plane the two are separated by an interface. Because of their lateral inhomogeneity, bridge phases can be exposed to a shear strain αs_x ($0 \leqslant \alpha \leqslant \frac{1}{2}$) by misaligning the substrates in the x-direction. Depending on the thermodynamic state of the confined fluid and details of the chemical decoration, shear-induced first-order phase transitions are feasible during which a bridge phase may be transformed into either a gaslike (evaporation) or a liquidlike phase (condensation). These phase transitions are studied by computing phase diagrams as functions of αs_x for a mean-field lattice-gas model. The lattice-gas calculations are amended by grand canonical ensemble Monte Carlo simulations of a fluid confined between chemically decorated substrate surfaces. The combination of the two sets of data reveals that the lattice-gas model captures correctly key characteristics of shear-induced first-order phase transitions in this rather complex system despite its mean-field character.

1. Introduction

In recent years a wealth of novel technologies have been devised by means of which solid surfaces can be decorated with geometrical or chemical structures in a controlled manner [1–6]. These structures are stable and can be fabricated on μm to nm length scales. Here we are concerned with *chemically* patterned substrates where the endowment of solid surfaces with such a pattern can be achieved by lithographic methods [2, 4] or wet chemical etching [1]. Microcontact printing is yet another method. Here one uses elastomer stamps and, in certain cases, subsequent wet chemical etching to imprint chemical structures on substrate surfaces [7–9].

Chemically decorated solid substrates play an important rôle in a variety of technologically important applications. One of these is in the field of 'microfluidics' [10, 11] where one modifies the wetting characteristics of an underlying substrate along chemical 'lanes', say, so that small portions of liquid can be transported through these lanes and across the substrate

† Author to whom any correspondence should be addressed.

0953-8984/00/081569+26$30.00

without spilling. At a different part of the substrate the fluid may then be analysed or subjected to chemical reactions [10, 11]. It is conceivable that if one endows a solid substrate with an integrated network of chemical nanostructures, these may function as chemical chips or minute chemical factories [11]. Another realization of a chemically decorated solid is the so-called 'Janus bead' which is a spherical colloidal particle with one hemisphere hydrophilic, the other one being hydrophobic [12, 13]. Along the equator the two portions have a rather sharp and well-defined junction. Janus beads can be considered as amphiphilic solids with a stabilizing effect on oil–water interfaces [12].

These examples may suffice to explain why there is also a still-increasing theoretical interest in the behaviour of soft condensed matter near chemically decorated solid substrates (see [14, 15] for recent reviews). From a theoretical perspective two key features of these systems have to be realized. First, the presence of *any* (planar) substrate breaks the symmetry and the system is no longer translationally invariant in all three spatial dimensions. This gives rise to surface-induced phase transitions, so-called wetting transitions which may be first or second order. At a first-order wetting transition the thickness of a fluid film adsorbed on a solid substrate diverges spontaneously at a temperature $T_w < T_x$ upon approaching bulk liquid–gas coexistence if the fluid wets the substrate (T_x: bulk coexistence temperature) (see [16–20] for reviews of wetting transitions at chemically homogeneous substrates). Second, nanoscopic chemical decoration of a substrate introduces new length scales in addition to the range of interactions among fluid molecules. These length scales are set by geometry and size of the chemical pattern and have an impact on both the wetting characteristics and the density profile of the adsorbed fluid as was recently demonstrated by Bauer and Dietrich on the basis of density functional calculations [21]. Details do, of course, depend on the chemical pattern imprinted on the substrate, the respective strength of the fluid–substrate interactions with the different substrate parts, and, last but not least, the chemical nature of the fluid wetting the substrate [22–26].

If the chemical pattern is not nanoscopic but on a μm length scale, one may employ phenomenological or square-gradient approaches [27–33] to study the morphology of liquids wetting chemically patterned substrates [31–33]. Consider, for example, a chemically striped substrate domain where the stripes are wetted by a liquid. Lipowsky *et al* showed that if one deposits a small amount of liquid on such a substrate it forms homogeneous channels over the stripes at first, eventually undergoing a transition to a 'bulge state' (see figure 5 in [34]), a morphology which was also observed experimentally using optical microscopy [27].

If the fluid is not interacting with just a single chemically decorated substrate but *confined* by two of them to spaces of microscopic or mesoscopic dimensions, confinement to such a nanoscopic slit adds an additional length scale to the problem. In general, the phase behaviour of a confined fluid differs markedly from that of its bulk counterpart even in cases where the substrates are composed of just a single atomic species (i.e., chemically homogeneous substrates) in that the coexistence curve $\mu_x^{lg}(T)$ is shifted to lower chemical potentials and the critical temperature appears to be depressed with respect to the bulk. These effects have been investigated in depth experimentally [35–40] and theoretically [41–48].

If, on the other hand, the confining substrates are planar but decorated with alternating strips of weakly and strongly adsorbing solid, Röcken and Tarazona were the first to point out that, in addition to liquid–gas coexistence, so-called 'bridge phases' may form as a third phase coexisting with either one of the other two or with both of them simultaneously (at a triple point) [49]. A bridge phase consists of two parts: a high(er)-density fluid spanning the space between the strongly adsorbing (and perfectly aligned) substrates and a low(er)-density fluid stabilized by its weakly adsorbing parts; the two density regimes are connected through an interface perpendicular to the confining (planar) substrates. The interface bears a resemblance

to the one at bulk liquid–gas coexistence [50]. Thus, bridge phases are inhomogeneous in the direction perpendicular to the interface. In the direction perpendicular to the substrate plane the high(er)-density portion of a bridge phase is stratified; that is, molecules arrange themselves in individual layers parallel with that plane. Coexistence between gaslike, liquidlike, and bridge phases depends crucially on the chemical corrugation of the decorated substrate—that is, on the relative widths of its weakly and strongly adsorbing parts [51, 52]. By virtue of the geometry of the substrates and the inhomogeneity of bridge phases, the latter can be exposed to shear strains by misaligning the former.

In a parallel publication [53] we explore the stress–strain relationship in *fluids* confined by chemically striped substrates and address the issue of thermodynamic stability. Within the framework of a mean-field lattice-gas model we also studied shear-strain-induced phase transitions between gaslike, liquidlike, and bridge phases [54]. The mean-field lattice gas is quite useful in this respect because it permits one to determine the phase diagram even for complex model systems at very little computational expense. However, it is not *per se* obvious that it is sufficiently realistic to capture all the subtleties of phase behaviour of confined fluids exposed to shear strain by, say, chemically decorated substrate surfaces. Therefore, it seems interesting to investigate in depth the reliability of the lattice-gas model by comparing its predictions with grand canonical ensemble Monte Carlo simulations for a related but more realistic model.

This paper, devoted to such an endeavour, is organized as follows. In section 2 we introduce the mean-field lattice-gas model of a fluid confined between chemically striped substrate surfaces and discuss the numerical procedure used to calculate its phase diagram. The corresponding continuous model is introduced in section 3. Section 4 is devoted to a presentation of results obtained for the two models with particular emphasis on the impact of shear strain. The paper ends in section 5 with a summary and a brief discussion of our main findings.

2. Mean-field lattice-gas model

2.1. Thermodynamics

For studying the phase behaviour in thermodynamically open systems, the grand potential Ω is a key quantity. In an inhomogeneous confined fluid, whose thermodynamic state may be specified conveniently by chemical potential μ and temperature T, $\Omega[\rho(\boldsymbol{r})]$ is a functional of the local density $\rho(\boldsymbol{r})$. For fixed T and μ the thermodynamically stable phase is characterized by that $\rho(\boldsymbol{r})$ which minimizes Ω. Thus, $\rho(\boldsymbol{r})$ is a solution of the variational equation

$$\frac{\delta\Omega[\rho(\boldsymbol{r})]}{\delta\rho(\boldsymbol{r})} = 0 \qquad \mu, T = \text{constant} \tag{1}$$

which may be solved at minimum computational expense by employing a lattice-gas model where

$$\Omega[\rho(\boldsymbol{r})] = \mathcal{F}[\rho(\boldsymbol{r})] + \sum_{\boldsymbol{r}}\{\Phi(\boldsymbol{r}) - \mu\}\rho(\boldsymbol{r}). \tag{2}$$

In (2), $\Phi(\boldsymbol{r})$ is the fluid–substrate potential and $\boldsymbol{r}$ is a site on a simple cubic lattice of $n_x \times n_y \times n_z$ nodes. Periodic boundary conditions are applied in the x- and y-directions. At mean-field level the (intrinsic) free-energy functional $\mathcal{F}$ is given by

$$\begin{aligned}\mathcal{F} &= \sum_{\boldsymbol{r}}\left(-\frac{\epsilon_{\mathrm{ff}}}{2}{\sum_{\boldsymbol{r}'}}'\rho(\boldsymbol{r})\rho(\boldsymbol{r}') + k_{\mathrm{B}}T\left\{\rho(\boldsymbol{r})\ln\rho(\boldsymbol{r}) + [1-\rho(\boldsymbol{r})]\ln[1-\rho(\boldsymbol{r})]\right\}\right) \\ &= \mathcal{U} - T\mathcal{S}\end{aligned} \tag{3}$$

as detailed in the appendix where k_B is Boltzmann's constant, ϵ_{ff} determines the strength of the fluid–fluid interaction, $\mathcal{U}$ and $\mathcal{S}$ are internal energy and entropy (functionals), respectively, and the sum on $\boldsymbol{r}'$ extends over the (six) nearest-neighbour lattice sites of $\boldsymbol{r}$, signified by the prime attached to the summation sign.

Various confinement scenarios are realized through different choices for $\Phi(\boldsymbol{r})$. In all cases the lattice gas is confined by two parallel substrates in the x–y plane (see figure 1). Each substrate is composed of different chemical species located in the ranges $1 \leqslant x \leqslant n_s$ and $n_s < x \leqslant n_x$ $(z = 1, n_z)$ whose interaction with the lattice gas is strongly (coupling constant ϵ_{fs}) or weakly (coupling constant ϵ_{fw}) attractive, respectively (see figure 1). The substrates may be misaligned in the x-direction which is effected by shifting the strongly attractive portion of the upper substrate by Δn_x lattice sites in the $+x$-direction. Thus, it is convenient to introduce a parameter $\alpha := \Delta n_x / n_x$ to specify the misalignment of the substrates quantitatively where $\{\alpha | 0 \leqslant \alpha \leqslant \alpha_{max}\}$. If n_x is even, $\alpha_{max} = 1/2$, whereas $\alpha_{max} = (n_x - 1)/2n_x$ if n_x is an odd number. If $\alpha = 0$ the substrates are 'in registry', i.e. strongly and weakly attractive portions of the two substrates are exactly opposite each other; $\alpha = \alpha_{max}$ if the misalignment is maximum (i.e., the substrates are 'out of registry'). This reflects the fact that only discrete values of α can be realized because of the discrete nature of the lattice. Thus, α is a measure of shear strain imposed on the confined lattice gas, affecting its phase behaviour via $\Phi(\boldsymbol{r}) = \Phi^{[1]}(\boldsymbol{r}) + \Phi^{[2]}(\boldsymbol{r})$ (see (2)) where

$$\Phi^{[1]}(\boldsymbol{r}) \equiv \Phi^{[1]}(x, z) = \begin{cases} \infty & & z < 1 \\ \left\{ \begin{array}{ll} -\epsilon_{fs} & 1 \leqslant x \leqslant n_s \\ -\epsilon_{fw} & n_s < x \leqslant n_x \end{array} \right\} & & z = 1 \\ 0 & & z > 1 \end{cases} \tag{4}$$

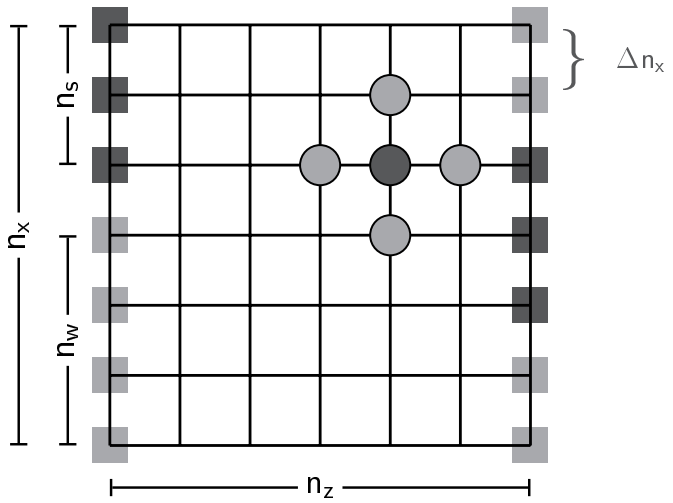

Figure 1. A schematic diagram of the lattice-gas model of a fluid confined between chemically corrugated substrates in the x–z plane. Each molecule (black circle) interacts with its nearest neighbours (grey circles). The two remaining nearest neighbours on the simple cubic lattice located at lattice sites in the translationally invariant y-direction perpendicular to the plane of the paper are not shown. Sites at which a lattice-gas molecule is subject to the substrate interaction $\Phi^{[k]}(\boldsymbol{r}) = -\epsilon_{fs}$ are shaded in dark grey (strongly attractive substrate portions, width n_s) whereas sites at which $\Phi^{[k]}(\boldsymbol{r}) = -\epsilon_{fw}$ (weakly attractive substrate portions, width $n_x - n_s$) are shaded in lighter grey (see (5), (4)). In the x-direction, periodic boundary conditions are applied (see the text).

represents the interaction with the lower substrate. Likewise

$$\Phi^{[2]}(\boldsymbol{r}) \equiv \Phi^{[2]}(x,z) = \begin{cases} \Phi^{[1]}(x-\alpha n_x, z) & \alpha n_x < x \leqslant n_x \\ \Phi^{[1]}(x-n_x(\alpha+1), z) & 0 < x \leqslant \alpha n_x \end{cases} \tag{5}$$

specifies the interaction with the upper substrate where the lattice sites are restricted to $\{(x,z)|1 \leqslant x \leqslant n_x, 1 \leqslant z \leqslant n_z\}$.

A special limiting case of the present model is the bulk lattice gas for which $\Phi^{[k]}(\boldsymbol{r}) \equiv 0$ and consequently $\rho(\boldsymbol{r}) \equiv \rho$ becomes nonlocal. Solutions of (1) are then distributed in the μ–T plane according to

$$\mu = k_{\mathrm{B}}T \ln\left(\frac{\rho}{1-\rho}\right) - 6\epsilon_{\mathrm{ff}}\rho \tag{6}$$

from which the bulk phase diagram, characterized by a critical point, can easily be determined analytically [55]. A straightforward calculation yields $\mu_{\mathrm{c}} = -3$, $T_{\mathrm{c}} = \frac{3}{2}$, and $\rho_{\mathrm{c}} = \frac{1}{2}$ for the critical chemical potential, temperature, and density, respectively. Here and henceforth we employ dimensionless units—that is, energies are given in units of ϵ_{ff}, temperatures in units of $\epsilon_{\mathrm{ff}}/k_{\mathrm{B}}$, and lengths in units of the lattice constant ℓ_{lg} as far as the lattice gas is concerned (see also section 4.1.2). From (6) it is also easy to verify [55] that the critical exponent $\beta = \frac{1}{2}$, as expected for a mean-field theory (see [56]).

2.2. Numerical procedure

To solve the variational expression (1) subject to (2)–(4) we use the Jacobi–Newton iteration technique [57], proceeding iteratively in an alternating sequence of 'local' and 'global' minimization steps. Let $\rho_i^j(\boldsymbol{r})$ be the local density at $\boldsymbol{r}$ in the ith local and jth global minimization step. A *local* estimate for the corresponding minimum value Ω_i^j is obtained via Newton's method:

$$\rho_{i+1}^j(\boldsymbol{r}) = \rho_i^j(\boldsymbol{r}) - \frac{f[\rho_i^j(\boldsymbol{r})]}{f'[\rho_i^j(\boldsymbol{r})]} \qquad i = 0, 1, 2, \ldots \tag{7}$$

where from (2) and (3)

$$f[\rho(\boldsymbol{r})] \equiv \frac{\delta\Omega[\rho(\boldsymbol{r})]}{\delta\rho(\boldsymbol{r})} = -k_{\mathrm{B}}T \ln\frac{\rho(\boldsymbol{r})}{1-\rho(\boldsymbol{r})} + \epsilon_{\mathrm{ff}} {\sum_{\boldsymbol{r}'}}' \rho(\boldsymbol{r}') + \mu + \sum_{k=1}^{2} \Phi^{[k]}(\boldsymbol{r}) \tag{8}$$

$$f'[\rho(\boldsymbol{r})] = -\frac{k_{\mathrm{B}}T}{\rho(\boldsymbol{r})[1-\rho(\boldsymbol{r})]}. \tag{9}$$

In (9), $f'(x) = \mathrm{d}f(x)/\mathrm{d}x$. It is important to realize that throughout each local minimization cycle, $\{\rho(\boldsymbol{r}')\}$ are maintained at the initial values assigned at the beginning of that cycle for all $\boldsymbol{r}$. The iterative solution of (7) is halted if $\max_r |\rho_{i+1}^j(\boldsymbol{r}) - \rho_i^j(\boldsymbol{r})| \leqslant 10^{-7}$ which is achieved in approximately 2–3 iterations. Local minimization is performed by visiting each lattice site consecutively; the local cycle ends once all sites have been considered.

'Global' minimization then involves updating the local density of the *entire* lattice according to $\rho_0^{j+1}(\boldsymbol{r}) = \rho_{i+1}^j(\boldsymbol{r})$, thus providing new initial values for the next *local* minimization cycle (by setting $j+1 \to j$ and returning to (7)). Global minimization is carried out until $\max_r |\rho_0^{j+1}(\boldsymbol{r}) - \rho_0^j(\boldsymbol{r})| \leqslant 10^{-7}$ which is achieved in roughly 100 steps.

To initiate the Newton–Jacobi iteration, suitable starting conditions have to be provided. Since (1) will generally have three structurally different solutions $\rho(\boldsymbol{r})$ (see figure 2(a),

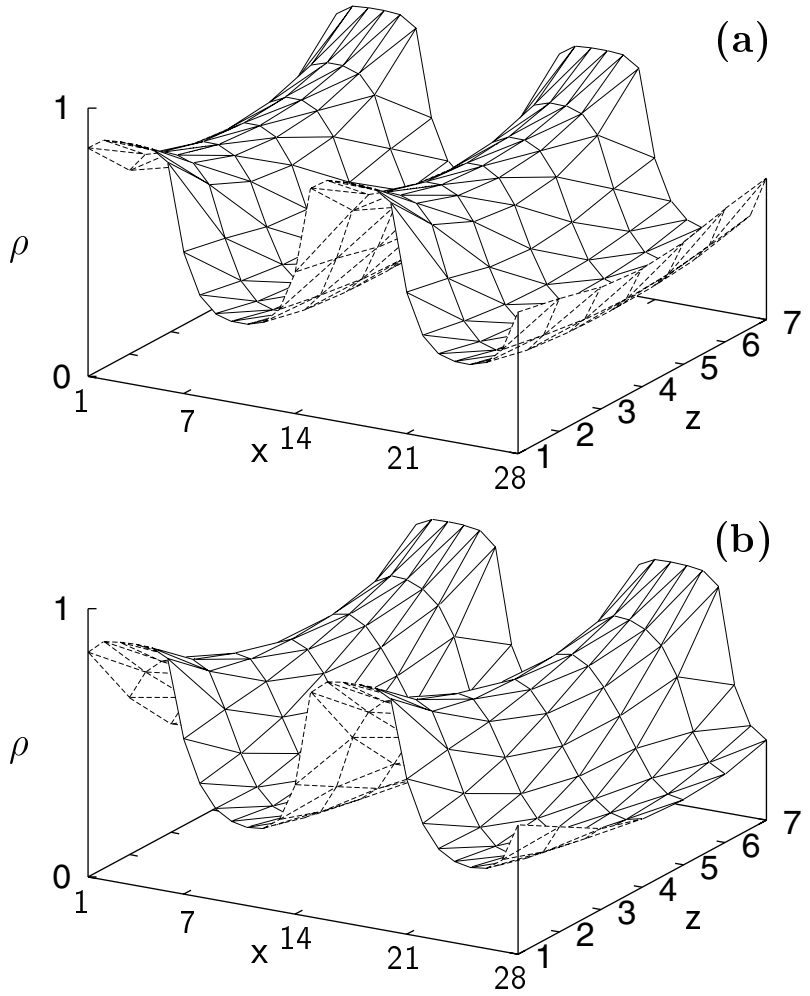

Figure 2. Local density $\rho(x, z)$ for a confined lattice at $T = 1.0$, $\mu = -3.036\,58$. The substrates are characterized by $n_x = 14$, $n_z = 7$, $n_w = 8$, $n_s = 6$, $\epsilon_{fw} = 0.4$, and $\epsilon_{fs} = 1.4$: (a) bridge phase ($\alpha = 0$); (b) bridge phase ($\alpha = \frac{5}{14}$); (c) gaslike phase ($\alpha = \frac{1}{2}$); (d) liquidlike phase ($\alpha = \frac{1}{2}$). The plots in (c) and (d) correspond to coexisting phases (see figure 9, later). Two periods of $\rho(x, z)$ in the x-direction are shown because of the periodicity of the lattice (see section 2.1).

figure 2(c), figure 2(d)), it proves sensible in practice to start from (see figure 1)

$$\rho_0^0(\boldsymbol{r}) = \begin{cases} \rho_l^{\text{init}} = 0.95 & \forall \boldsymbol{r} \\ \rho_b^{\text{init}} = \begin{cases} 0.95 & \begin{cases} 1 \leqslant x \leqslant n_s & z = 1 \\ 1 + \alpha n_x \leqslant x \leqslant n_s + \alpha n_x & z = n_z \\ 1 + \alpha n_x \leqslant x \leqslant n_s & 2 \leqslant z \leqslant n_z - 1 \end{cases} \\ 0.05 & \text{otherwise} \end{cases} \\ \rho_g^{\text{init}} = 0.05 & \forall \boldsymbol{r} \end{cases} \tag{10}$$

because $0 \leqslant \rho(\boldsymbol{r}) \leqslant 1$ (periodic boundary conditions!). After convergence of the Jacobi–Newton iteration, the grand potentials for gaslike ($\Omega^g[\rho_g(\boldsymbol{r})]$; see figure 2(c)), liquidlike ($\Omega^l[\rho_l(\boldsymbol{r})]$; see figure 2(d)), and so-called 'bridge phases' ($\Omega^b[\rho_b(\boldsymbol{r})]$; see figure 2(a)) will

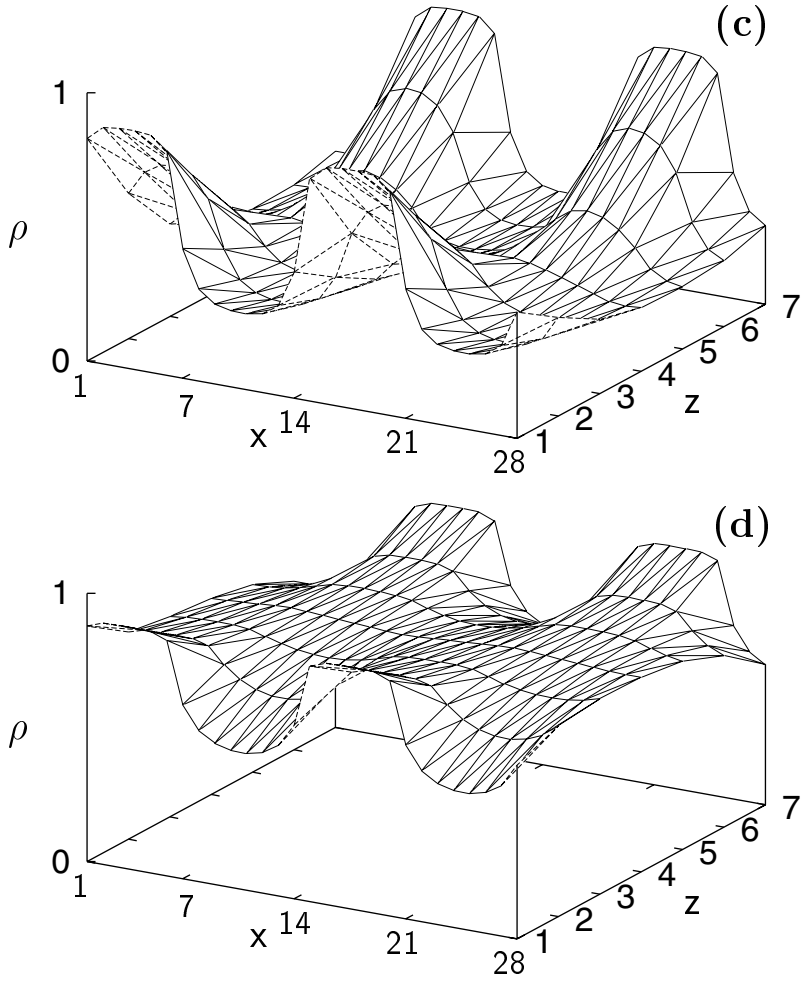

Figure 2. (Continued)

differ in general. We emphasize that in our terminology 'bridge phase' refers to the *entire* morphology illustrated by the plot in figure 2(a). Consequently, the term 'bridge phase' must not be confused with a high(er)-density phase in thermodynamic equilibrium with a low(er)-density phase, the two being separated by an interface. Because $(\partial\Omega^{\mathrm{l}}/\partial\mu)_T < (\partial\Omega^{\mathrm{b}}/\partial\mu)_T < (\partial\Omega^{\mathrm{g}}/\partial\mu)_T$ one expects intersections $\{\mu^{\mathrm{gl}}, T\}$, $\{\mu^{\mathrm{gb}}, T\}$, and $\{\mu^{\mathrm{bl}}, T\}$ to exist, defined such that $\Omega^{\mathrm{gl}} = \Omega^{\mathrm{g}}[\rho_{\mathrm{g}}(\boldsymbol{r})] = \Omega^{\mathrm{l}}[\rho_{\mathrm{l}}(\boldsymbol{r})]$, $\Omega^{\mathrm{gb}} = \Omega^{\mathrm{g}}[\rho_{\mathrm{g}}(\boldsymbol{r})] = \Omega^{\mathrm{b}}[\rho_{\mathrm{b}}(\boldsymbol{r})]$, and $\Omega^{\mathrm{bl}} = \Omega^{\mathrm{b}}[\rho_{\mathrm{b}}(\boldsymbol{r})] = \Omega^{\mathrm{l}}[\rho_{\mathrm{l}}(\boldsymbol{r})]$, respectively. Therefore, corresponding pairs of structures $\{\rho_{\mathrm{g}}(\boldsymbol{r}), \rho_{\mathrm{l}}(\boldsymbol{r})\}$, $\{\rho_{\mathrm{g}}(\boldsymbol{r}), \rho_{\mathrm{b}}(\boldsymbol{r})\}$, and $\{\rho_{\mathrm{b}}(\boldsymbol{r}), \rho_{\mathrm{l}}(\boldsymbol{r})\}$ may be perceived as coexisting phases (not necessarily in thermodynamic equilibrium; see below). In practice, two scenarios have to be distinguished:

(i) $T < T_{\mathrm{tr}}$: $\mu^{\mathrm{bl}} < \mu^{\mathrm{gl}} < \mu^{\mathrm{gb}}$ and $\Omega^{\mathrm{bl}} > \Omega^{\mathrm{gl}} > \Omega^{\mathrm{gb}}$ such that for sufficiently low temperatures only gaslike (see figure 2(c)) and liquidlike phases (see figure 2(d)) coexist. The set of points $\{\mu^{\mathrm{gl}}, T\}$ defines the coexistence curve $\mu_{\mathrm{x}}^{\mathrm{gl}}(T)$.

(ii) $T > T_{\mathrm{tr}}$: $\mu^{\mathrm{bl}} > \mu^{\mathrm{gl}} > \mu^{\mathrm{gb}}$ and $\Omega^{\mathrm{bl}} < \Omega^{\mathrm{gl}} < \Omega^{\mathrm{gb}}$. The set $\{\mu^{\mathrm{gb}}, T\}$ defines the curve $\mu_{\mathrm{x}}^{\mathrm{gb}}(T)$ along which gaslike and bridge phases coexist, whereas the set $\{\mu^{\mathrm{bl}}, T\}$ defines

the coexistence curve $\mu_x^{bl}(T)$ for bridge and liquidlike phases; because $\mu_x^{gb}(T) \neq \mu_x^{bl}(T)$, the separately coexisting bridge phases will generally have different $\rho_b(\boldsymbol{r})$. Coexisting gaslike and liquidlike phases are metastable.

Scenarios (i) and (ii) imply existence of a triple point $\{\mu_{tr}, T_{tr}\}$ at which all three phases coexist—that is, $\mu_x^{bl}(T) = \mu_x^{gl}(T) = \mu_x^{gb}(T)$ and $\Omega^{bl} = \Omega^{gl} = \Omega^{gb}$. Because of (ii) one also expects two critical points, $\{\mu_c^{gb}, T_c^{gb}\}$ and $\{\mu_c^{bl}, T_c^{bl}\}$, defined such that at Ω^{gb}, $(\partial\Omega^g/\partial\mu)_{T=T_c^{gb}} = (\partial\Omega^b/\partial\mu)_{T=T_c^{gb}}$ and at Ω^{bl}, $(\partial\Omega^b/\partial\mu)_{T=T_c^{bl}} = (\partial\Omega^l/\partial\mu)_{T=T_c^{bl}}$. In other words, $\rho_g(\boldsymbol{r}) = \rho_b(\boldsymbol{r})$ at $\{\mu_c^{gb}, T_c^{gb}\}$ and $\rho_b'(\boldsymbol{r}) = \rho_l(\boldsymbol{r})$ at $\{\mu_c^{gb}, T_c^{gb}\}$ (where $\rho_b(\boldsymbol{r}) \neq \rho_b'(\boldsymbol{r})$ in general).

To determine $\mu_x^{gl}(T)$, $\mu_x^{gb}(T)$, and $\mu_x^{bl}(T)$ we take advantage of the monotonicity of $(\partial\Omega/\partial\mu)_T$ and compute $\Omega^g(\mu)$ and $\Omega^l(\mu)$ for a sufficiently low temperature $T \ll T_{tr}$ and two chemical potentials $\mu_1 < \mu_2$ via the Jacobi–Newton method. Approximating $\Omega^l(\mu)$ and $\Omega^g(\mu)$ in the interval $[\mu_1, \mu_2]$ by straight lines permits us to compute a first estimate $\mu^{gl} \equiv \mu^{[1]}$ of the chemical potential at phase coexistence from $\widetilde{\Omega}^g(\mu^{[1]}) = \widetilde{\Omega}^l(\mu^{[1]})$ where we use the tilde to indicate the linear approximation to the grand potential curves. However, the grand potentials do not depend linearly on μ as reflected by $\Omega^g(\mu^{[1]}) \neq \Omega^l(\mu^{[1]})$, and the initial guess $\mu^{[1]}$ needs to be improved. This can be achieved by considering subintervals $[\mu_1, \mu^{[1]}]$ or $[\mu^{[1]}, \mu_2]$ depending on whether $|\mu_1 - \mu^{[1]}| < |\mu_2 - \mu^{[1]}|$ or $|\mu_1 - \mu^{[1]}| > |\mu_2 - \mu^{[1]}|$, respectively. Approximating in the refined interval both $\Omega^g(\mu)$ and $\Omega^l(\mu)$ by straight lines, as before, permits us to compute an improved estimate $\mu^{[2]}$ of the chemical potential at phase coexistence. The refinement procedure is repeated until $|\Omega^g(\mu^{[k]}) - \Omega^l(\mu^{[k]})| \leqslant 10^{-7}$ which is usually achieved in $k = 2$–4 refinement steps.

With the final estimate of μ^{gl} we compute $\rho_b(\boldsymbol{r})$ via the Jacobi–Newton technique and calculate $\Omega^b[\rho_b(\boldsymbol{r})]$ from (2) and (3). Again, two scenarios have to be distinguished:

(i) $\Omega^b > \Omega^{gl}$; the bridge phase is metastable. Thus, gaslike and liquidlike phases coexist along $\mu_x^{gl}(T)$ and we can repeat the calculation as described for the next temperature $T' := T + \Delta T$ ($\Delta T = 0.01$). At T' the starting solution $\rho_0^0(\boldsymbol{r})$ for all three phases is taken to be the corresponding one obtained for the preceding temperature T.

(ii) $\Omega^b < \Omega^{gl}$; the bridge phase is thermodynamically stable in the range $\mu^{gb} \leqslant \mu \leqslant \mu^{bl}$, and the curves $\mu_x^{gb}(T)$ and $\mu_x^{bl}(T)$ need to be determined separately by the refinement procedure described above.

As the critical point(s) is (are) approached, the identification of coexisting phases becomes increasingly difficult because their $\Omega(\mu)$s are nearly identical. Therefore, we refine the temperature interval such that $\Delta T = 2.5 \times 10^{-3}$ if the difference between the densities of coexisting phases $\Delta\rho \lesssim 0.05$.

3. Continuous model

3.1. The fluid–substrate potential

The continuous analogue of the lattice-gas model consists of a film composed of spherically symmetric molecules sandwiched between the surfaces of two solid substrates. The substrate surfaces are planar, parallel, and separated by a distance s_z along the z-axis of the coordinate system. The substrates are semi-infinite in the z-direction, occupying the half-spaces $s_z/2 \leqslant z \leqslant \infty$ and $-\infty \leqslant z \leqslant -s_z/2$, and are infinite in the x- and y-directions. Each substrate comprises slabs of two types: strongly adsorbing and weakly adsorbing. The 'strong' and 'weak' slabs have widths d_s and $d_w/2$, respectively, in the x-direction and are infinite in the

y-direction. If the substrates are aligned as in figure 3 the system is thus periodic in the x-direction with period $s_x = d_s + d_w$ and its properties are translationally invariant in the y-direction. In practice we take the system to be a finite piece of the film, imposing periodic boundary conditions [58] on the planes $x = \pm s_x/2$ and $y = \pm s_y/2$ where s_α ($\alpha = x, y$) is the side length of the system in the α-direction. To emphasize the continuous nature of the present model we introduce different notation as far as the characteristic dimensions are concerned (i.e., $s_x \leftrightarrow n_x$, $s_y \leftrightarrow n_y$, $s_z \leftrightarrow n_z$, and $d_s \leftrightarrow n_s$).

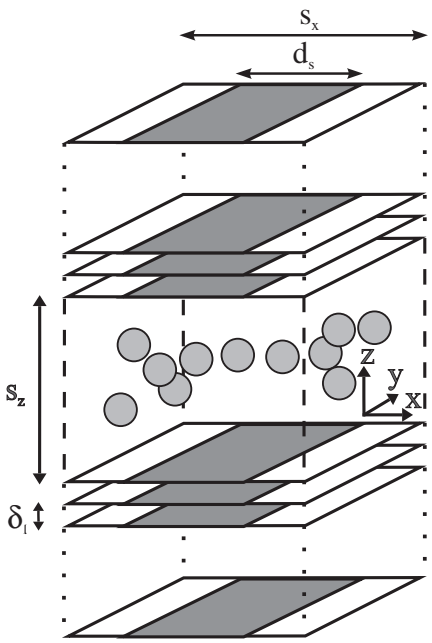

Figure 3. A schematic diagram of a simple fluid confined by a chemically heterogeneous model pore. Fluid molecules (grey spheres) are spherically symmetric. Each substrate consists of a sequence of crystallographic planes separated by a distance δ_ℓ along the z-axis. The surface planes of the two opposite substrates are separated by a distance s_z. Periodic boundary conditions are applied in the x- and y-directions (see the text).

Substrate atoms forming the two slabs are assumed to be of the same 'diameter' σ and to occupy sites of the face-centred cubic (fcc) lattice (the substrate surfaces are (100) planes) where the lattice constant ℓ is the same for the atomic species in both strong and weak slabs. Thus, substrate atoms forming these slabs are distinguished only by their respective strength of interaction with film molecules. We assume the total potential energy to be a sum of pairwise-additive Lennard-Jones (LJ) (12, 6) (-type) potentials $u(r)$ (see section 4.1.2). For the interaction between a pair of film molecules, the potential-well depth $\epsilon = \epsilon_{ff}$ (i.e., $u_{ff}(r)$). The nanoscale heterogeneity of the substrate is characterized by $\epsilon = \epsilon_{fs}$ (i.e., $u_{fs}(r)$) for the interaction of a fluid molecule with a substrate atom in the strong (central) slab, and by $\epsilon = \epsilon_{fw}$ (i.e., $u_{fw}(r)$) for the interaction of a fluid molecule with a substrate atom in either of the two weak (outer) slabs (see figure 3). We take $\epsilon_{fs}/\epsilon_{ff} = 1.25$ and $\epsilon_{fw}/\epsilon_{ff} = 10^{-3}$.

Since we are concerned with the effects of nanoscale chemical decoration on the behaviour of a confined fluid, we expect details of the substrate structure not to matter greatly at the atomic level. Therefore, we adopt a mean-field representation of the interaction of a fluid molecule with the substrate, which we obtain by averaging the fluid–substrate interaction potential over

positions of substrate atoms in the x–y plane. The resulting mean-field potential can be expressed as [50–52]

$$\Phi^{[k]} = -3\pi\left(\frac{\sigma}{\ell}\right)^2 \sum_{m=-\infty}^{\infty}\sum_{m'=0}^{\infty}\left\{(\epsilon_{\mathrm{fw}}-\epsilon_{\mathrm{fs}})\left[\Delta\left(\widetilde{x}+\frac{d_{\mathrm{s}}}{2}-ms_x,\,\frac{s_z}{2}+m'\delta_\ell\pm z\right)\right.\right.$$
$$\left.-\Delta\left(\widetilde{x}-\frac{d_{\mathrm{s}}}{2}-ms_x,\,\frac{s_z}{2}+m'\delta_\ell\pm z\right)\right]$$
$$-\epsilon_{\mathrm{fw}}\left[\Delta\left(\widetilde{x}+\frac{s_x}{2}-ms_x,\,\frac{s_z}{2}+m'\delta_\ell\pm z\right)\right.$$
$$\left.\left.-\Delta\left(\widetilde{x}-\frac{s_x}{2}-ms_x,\,\frac{s_z}{2}+m'\delta_\ell\pm z\right)\right]\right\} \tag{11}$$

where δ_ℓ is the spacing between successive crystallographic planes in the $\pm z$-direction. The sign is chosen according to the convention $+ \leftrightarrow k = 1$ and $- \leftrightarrow k = 2$. In (11) the auxiliary function Δ is defined as (see [51] for details)

$$\Delta(x'', z'') := \frac{21}{32} I_3(x'', z'') - I_4(x'', z'') \tag{12}$$

where

$$I_3(x'', z'') = \frac{x''\sigma^{10}}{9z''^2\sqrt{R^9}}\left[1+\frac{8}{7}S+\frac{48}{35}S^2+\frac{64}{35}S^3+\frac{128}{35}S^4\right] \tag{13}$$

$$I_4(x'', z'') = \frac{x''\sigma^4}{3z''^2\sqrt{R^3}}[1+2S]. \tag{14}$$

Here $R := x''^2 + z''^2$ and $S := R/x''^2$. To evaluate the fluid–substrate interaction we set up a two-dimensional grid and compute Φ prior to the simulation at the nodes of this grid. According to the actual position of a fluid molecule (not necessarily coinciding with one of the nodes), Φ is calculated during the simulation by bilinear interpolation as detailed in [51,52].

Because of the chemical decoration of each substrate, a confined fluid can be exposed to a shear strain by misaligning the substrates in the $+x$-direction according to

$$\widetilde{x} := \begin{cases} x & k = 1 \\ x - \alpha s_x & k = 2 \end{cases} \tag{15}$$

where $\alpha := \delta_\alpha/s_x$ is a dimensionless number and δ_α is the magnitude of the relative displacement of the substrates with respect to each other where $\{\alpha | 0 \leqslant \alpha \leqslant \frac{1}{2}\}$ may vary continuously between its limits (see section 2.1); $\alpha = 0$ refers to substrates in registry whereas $\alpha = \frac{1}{2}$ if the substrates are out of registry.

3.2. Thermodynamics

We treat the confined fluid as a thermodynamically open system. Hence, equilibrium states correspond to minima of the grand potential $\Omega := \mathcal{F} - \mu N$. With the aid of Gibbs' fundamental equation [59] one obtains

$$\mathrm{d}\Omega = -\mathcal{S}\,\mathrm{d}T - N\,\mathrm{d}\mu + T_{xx}s_y s_z\,\mathrm{d}s_x + T_{yy}s_x s_z\,\mathrm{d}s_y + T_{zz}s_x s_y\,\mathrm{d}s_z + T_{zx}s_x s_y\,\mathrm{d}(\alpha s_x). \tag{16}$$

In (16), $T_{\alpha\alpha}$ ($\alpha = x, y, z$) is a diagonal element of the stress tensor $\mathbf{T}$; T_{zx} is the shear stress—that is, the x-component of the force acting on the z-directed area $A := s_x s_y$, and αs_x is

the conjugate shear strain. By convention, $T_{\alpha\beta} < 0$ if the β-component of the force exerted by the film on the α-directed area points outward. Because the fluid–substrate potential is translationally invariant in the y-direction, $T_{zy} \equiv 0$. According to the definition of $\mathbf{T}$, the remaining four off-diagonal components T_{xz}, T_{yz}, T_{xy}, and T_{yx} vanish since the substrates are rigid and cannot be compressed or sheared.

From (16) it is evident that Ω depends on the set $\{T, \mu, s_x, s_y, s_z, \alpha s_x\}$ of natural variables. Furthermore, since the fluid–substrate potential is translationally invariant in the y-direction, Ω is a homogeneous function of degree one in s_y provided that T, μ, s_x, s_z, and αs_x are fixed. Under these conditions, Euler's theorem applies and one obtains

$$\Omega = T_{yy} A s_y := T_{yy} V \qquad \text{fixed } T, \mu, s_x, s_y, \alpha s_x \tag{17}$$

where we take the zero of Ω to coincide with $s_y = 0$ and V is the volume. Thus, equation (17) permits us to interpret T_{yy} as a grand potential density. Equation (17) is useful for distinguishing between thermodynamically stable and metastable states realized in grand canonical ensemble Monte Carlo simulations (see section 4.1.2). However, for this purpose a molecular expression for T_{yy} is required. It is given in (29) of [51] where we emphasize that there is no fluid–substrate contribution because Φ in (11) does not depend on the y-coordinate of a fluid molecule—that is, Φ is translationally invariant in this direction.

4. Results

4.1. Substrates in registry

4.1.1. Lattice gas. The primary result of (1) is the local density $\rho(\boldsymbol{r}) \equiv \rho(x, z)$ of the confined lattice gas. Because of the discrete nature of the model, $\rho(x, z)$ is defined only at lattice sites. However, to visualize $\rho(x, z)$ it proves convenient to interpolate between neighbouring sites. Figure 2(a) shows the typical structure of a bridge phase, namely a high(er) density over the strongly attractive portions of the substrate alternating in the x-direction with a low(er)-density regime over the weakly attractive ones. In the z-direction high(er)- and low(er)-density portions of the fluid span the entire space between the substrates with comparatively little variation of $\rho(x, z)$ along x = constant cuts. Under suitable thermodynamic conditions a bridge phase may condense and form a liquidlike phase. Alternatively, a bridge phase may evaporate leaving behind a gaslike phase.

Because of the different microscopic structures, one anticipates a rather complex phase diagram for a lattice gas confined between chemically decorated substrates which we determine according to the procedure described in section 2.2. Figure 4(a) shows plots of the coexistence curves in μ–T projection for various degrees of confinement (i.e., n_z). The horizontal line represents the bulk coexistence curve $\mu_x^{gl}(T) = \mu_c$ (see (6)) which we include for comparison. Along $\mu_x^{gl}(T)$, gas and liquid (bulk) phases coexist. Thus, the thermodynamic states $\Gamma^l = \{(\mu, T) | \mu > \mu_c, T \leqslant T_c\}$ belong to the one-phase liquid regime whereas the states $\Gamma^g = \{(\mu, T) | \mu < \mu_c, T \leqslant T_c\}$ pertain to the one-phase gas region. Consequently, $\mu_x^{gl}(T)$ is a line of first-order phase transitions terminating, of course, at $T = T_c$.

More subtle effects are observed if the lattice gas is confined by solid substrates, as plots in figure 4(a) show. For sufficiently large n_z, chemical decoration of the substrate does not matter but confinement effects prevail. For example, for $n_z = 15$ the critical point is shifted to (μ_c^{gl}, T_c^{gl}) where T_c^{gl} and μ_c^{gl} are lower than the bulk values T_c and μ_c. Moreover, $\mu_x^{gl}(T)$ is no longer parallel with the temperature axis as in the bulk.

If n_z decreases, a bifurcation appears at $T = T_{tr}$. Only (inhomogeneous) liquidlike and gaslike phases coexist along the line $\mu_x^{gl}(T)$ $(T < T_{tr})$. At $T = T_{tr}$ the latter two are in

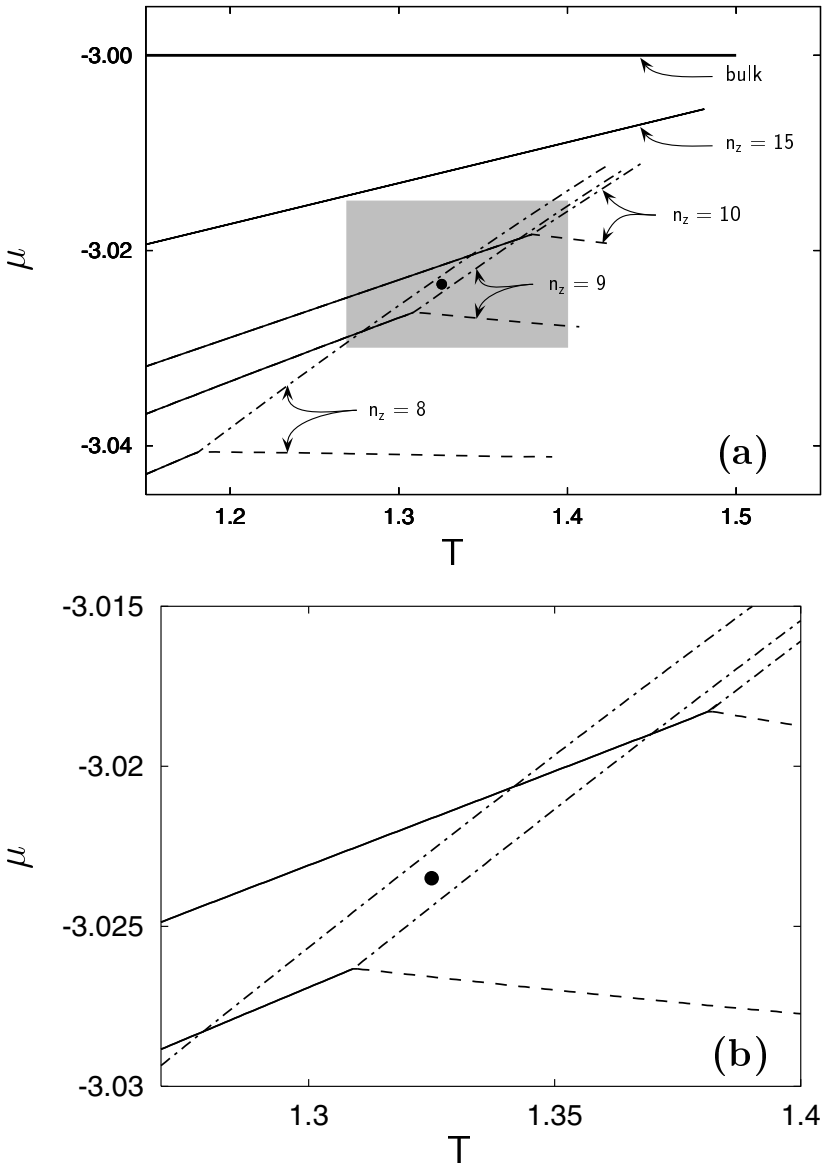

Figure 4. (a) Coexistence curves in T–μ projection for various confined lattice gases as functions of substrate separation n_z indicated in the figure ($\alpha = 0$, $n_x = 14$, $n_s = 8$, $\epsilon_{fs} = 1.4$, $\epsilon_{fw} = 0.3$); ——: $\mu_x^{gl}(T)$; – – –: $\mu_x^{gb}(T)$; — · —: $\mu_x^{bl}(T)$. The corresponding bulk coexistence curve is also shown. (b) As (a), but on an enhanced scale showing only the coexistence-curve branches in the grey box in (a); ● marks the fixed thermodynamic state of the confined fluid $T = 1.325$, $\mu = -3.0235$.

thermodynamic equilibrium with a bridge phase. For $T > T_{tr}$ the coexistence curve consists of two branches. The upper one, $\mu_x^{bl}(T)$, can be interpreted as a line of first-order phase transitions involving liquidlike and bridge phases whereas the lower one, $\mu_x^{gb}(T)$, corresponds to bridge and gaslike phases, respectively. Both branches terminate at their respective critical points $\{\mu_c^{bl}, T_c^{bl}\}$ and $\{\mu_c^{gb}, T_c^{gb}\}$. The entire coexistence curve $\mu_x(T)$ of the lattice gas is

formed by $\mu_x^{gl}(T)$, $\mu_x^{gb}(T)$, $\mu_x^{bl}(T)$, and the point $\{\mu_{tr}, T_{tr}\}$. Phase diagrams of this general type have to be expected also in cases where the substrate is geometrically instead of chemically corrugated [60]. We have verified numerically that

$$\lim_{T \to T_c^{ij}} \Delta\bar{\rho}_x^{ij} \propto (T_c^{ij} - T)^{\beta_{ij}} \geqslant 0 \tag{18}$$

where $\Delta\bar{\rho}_x^{ij}$ is the average-density difference between coexisting phases i and j. For the critical exponents we obtain $\beta_{gb} \simeq \beta_{bl} \simeq \frac{1}{2}$ within numerical accuracy for our three-dimensional lattice-gas model (see figure 1, section 2.1), indicating that the mean-field character is preserved at both critical points.

Comparing in figure 4(a) coexistence curves for $n_z = 8$ and 9 it is evident that the triple point is lowered further the more severe the confinement is, that is the smaller n_z is. Simultaneously, μ_c^{bl} increases whereas μ_c^{gb} decreases such that the one-phase region for bridge phases widens. Because of these rather complex variations of $\mu_x(T)$ with n_z it is conceivable that for a fixed thermodynamic state $\{\mu, T\}$ the confined phase is gaslike initially if n_z is sufficiently large. Upon lowering n_z, this gaslike phase may condense to a bridge and eventually to a liquidlike phase at even smaller n_z. This is illustrated in figure 4(b) for a specific thermodynamic state determined by $T = 1.325$ and $\mu = -3.0235$. From the plot it is clear that for $n_z \geqslant 10$ the confined fluid is gaslike because its thermodynamic state lies *below* all branches of $\mu_x(T)$. As the substrate separation decreases, however, one notices from the plot corresponding to $n_z = 9$ that the same thermodynamic state now pertains to the one-phase regime of liquidlike phases; that is, it falls *above* all branches of $\mu_x(T)$. Thus, in going from $n_z = 10$ to $n_z = 9$ the confined lattice gas underwent a first-order phase transition from a gaslike to a liquidlike phase. For an even smaller substrate separation $n_z = 8$, one sees from figure 4(a) that the triple point has shifted to rather small $\{\mu_{tr}, T_{tr}\}$ and that the one-phase region of bridge phases has widened considerably. Thus, as can be seen from the parallel figure 4(b), the thermodynamic state eventually belongs to the one-phase region of bridge phases where it remains for all smaller n_z. Hence, as one decreases the substrate separation from $n_z = 9$ to $n_z = 8$ an originally liquidlike phase is transformed into a bridge phase during a first-order phase transition.

A general feature of first-order phase transitions is release (or absorption) of latent heat which may be cast quantitatively in terms of the (molar) enthalpy of vaporization

$$\Delta h_v^{ij} := T(s_x^i - s_x^j) \geqslant 0 \tag{19}$$

of coexisting phases i and j. In (19), s_x^i and s_x^j are the associated molar entropies at coexistence. From (3) we deduce

$$s_x^i = -\frac{k_B}{n_x n_y n_z} \sum_{\boldsymbol{r}} \left\{ \ln \rho_x^i(\boldsymbol{r}) + \frac{1 - \rho_x^i(\boldsymbol{r})}{\rho_x^i(\boldsymbol{r})} \ln[1 - \rho_x^i(\boldsymbol{r})] \right\} \tag{20}$$

where $\rho_x^i(\boldsymbol{r})$ is the local density of phase i at coexistence. Thus, Δh_v^{ij} is a measure of the 'width' of the coexistence curve for phases i and j in T–ρ projection. According to this interpretation it is not surprising that Δh_v^{gl} for the bulk lattice gas in figure 5 decreases with increasing T, where $\Delta h_v^{gl} = 0$ for $T = T_c$ because gas and liquid phases become indistinguishable at the critical point. A parallel plot for the confined lattice gas shows that Δh_v^{gl} is smaller than its bulk counterpart for $T \leqslant T_{tr}$ because densities of gaslike and liquidlike phases are closer to each other under confinement. For $T = T_{tr}$, $\Delta h_v^{gl} = \Delta h_v^{gb} + \Delta h_v^{bl}$ as it must. For $T > T_{tr}$, Δh_v^{gl} is no longer defined for the confined lattice gas and Δh_v^{gb} and Δh_v^{bl} decrease with increasing T, eventually vanishing separately at the respective critical temperatures T_c^{gb} and T_c^{bl} (see figure 5).

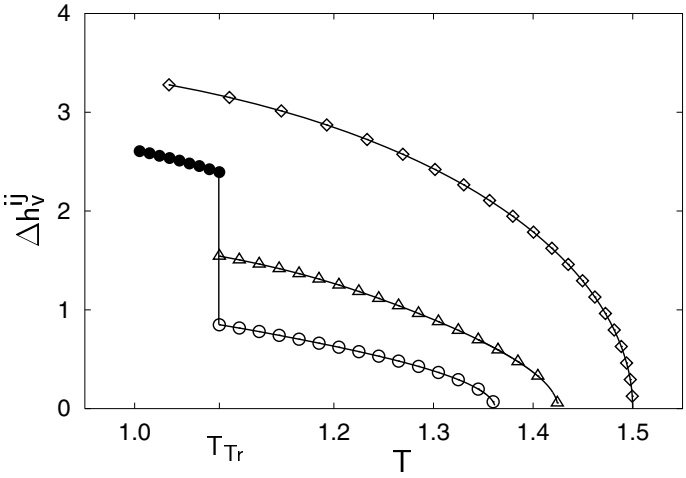

Figure 5. Molar enthalpy of vaporization Δh_v^{ij} as a function of temperature T; curves are shown for bulk (◇), i = g, j = l, and confined lattice gas ($\alpha = 0$, $n_x = 14$, $n_s = 6$, $n_z = 7$, $\epsilon_{fs} = 1.6$, $\epsilon_{fw} = 0.4$) where: i = g, j = l (●); i = g, j = b (○); i = b, j = l (△).

4.1.2. Continuous model. Parallel results for the continuous model were obtained assuming the confined fluid to be composed of argon atoms. As before for the lattice gas we express all quantities in the customary dimensionless (i.e., 'reduced') units. However, here we deviate from the lattice gas case by expressing length in units of σ.

Equilibrium properties of the confined fluid are obtained in Monte Carlo simulations in the grand canonical ensemble employing the algorithm proposed by Adams [61]. These simulations yield a sequence of M configurations $\{\boldsymbol{r}_k^N\}_{k=1,\ldots,M}$ minimizing Ω. Disregarding details, this procedure is therefore equivalent to solving (1). However, instead of using in the simulations the 'full' Lennard-Jones (LJ) (12, 6) potential (see section 3.1) to describe the fluid–fluid interaction, we employ a 'shifted-force' version defined such that the LJ (12, 6) potential and its first derivative vanish at the cut-off radius $r_c = 2.5$ [58]. As pointed out in [62], the shifted-force potential is advantageous because no long-range correction has to be applied to the fluid–fluid interaction since u_{ff} vanishes by definition for all $r \geqslant r_c$. This is particularly important in the present case where the Monte Carlo algorithm involves changes in the number of molecules [61] because μ is one of the thermodynamic state variables. The associated density change of $\pm 1/N$ between pairs of consecutive trial configurations would require an analytic energy correction during the generation of the Markov chain as far as the full (i.e., infinitely long-range) LJ (12, 6) potential is concerned. While explicit expressions for correction terms are available for the present slit-pore geometry [63], their application is not unproblematic under all circumstances [64].

Depending on the thermodynamic state, a fluid in the continuous model may form a gas-like, liquidlike, or bridge phase similar to the confined lattice gas (see figure 2, section 4.1.1). Typical structures of these three phases are illustrated by the plots in figure 6. As in figure 2(a) the plot of the local density $\rho(x, z)$ in figure 6(a) shows a typical bridge phase. For $\alpha = 0$, $\rho(x, z)$ is symmetric with respect to $x = 0$ and $z = 0$ as it must be (see figure 6(a)). As in the lattice-gas model, a bridge phase may condense or evaporate upon varying the thermodynamic conditions. The microscopic structure of liquidlike and gaslike phases in the absence of a shear strain is illustrated by the plots in figure 2(b) and figure 2(c) of [52]. From the plot in figure 6(a) one notices that $\rho(x, z)$ is a nonmonotonic function of z along any cut x = constant

in the high(er)-density regime. Nonmonotonicity of the local density is more clearly visible in the plot of contour lines of $\rho(x, z)$ (i.e., lines along which $\rho(x, z) =$ constant) in the parallel figure 7(a) showing a sequence of 'islands' in the z-direction surrounded by a closed line of lower density. This indicates that the enclosed higher-density regimes of bridge phases are well separated by a distance $\Delta z \simeq 1$ between centres of neighbouring islands. Thus, it is plausible to associate these islands with molecular strata parallel with the confining substrates. Stratification reflects substrate-mediated intermolecular correlations. It is therefore sensible that the parallel plot in figure 2(a) does not exhibit stratification because such correlations are explicitly disregarded at mean-field level (see (A.2)). With increasing distance from a substrate, stratification diminishes in the continuous model (see figure 6(a)) due to the decay of the fluid–substrate potential. This is reflected by a declining amplitude of oscillations in $\rho(x, z)$ with increasing distance from a substrate which can also be seen in figure 7(a) where the islands shrink in the transverse (i.e., x-) direction as $|z| \to 0$.

In the continuous model a confined fluid may undergo phase transitions between gaslike, liquidlike, and bridge phases similar to those observed for the confined lattice gas in section 4.1.1. To demonstrate the close correspondence between the two models as far as the phase behaviour is concerned we calculate the average overall density

$$\bar{\rho} := \frac{1}{s_x s_z} \int_{-s_x/2}^{s_x/2} \mathrm{d}x \int_{-s_z/2}^{s_z/2} \mathrm{d}z \; \rho(x, z) = \frac{\langle N \rangle}{V} \tag{21}$$

for various substrate separations s_z. The plot of $\bar{\rho}$ in figure 8 exhibits two discontinuities. From a parallel analysis of $\rho(x, z)$, the one around $s_z \simeq 8.2$ turns out to correspond to a first-order phase transition involving gaslike and liquidlike phases whereas the one at $s_z \simeq 7.5$ relates to a transition between a liquidlike phase and a bridge phase (upon reducing s_z). Therefore, the sequence of phase transitions in figure 8 resembles closely the scenario observed for the lattice gas in figure 4(b). However, depending on the precise chemical structure of these surfaces, different phase transitions are possible (see figure 10 in [52]), which can also be explained qualitatively within the framework of the mean-field lattice gas. Oscillations of $\bar{\rho}$ in figure 8 over the range $2 \lesssim s_z \lesssim 6$ reflect stratification of the confined fluid as described above.

However, investigations of phase transitions by means of Monte Carlo simulations in the grand canonical ensemble are frequently plagued by metastability—that is, the existence of a sequence of configurations $\{\boldsymbol{r}_k^N\}_{k=1,\ldots,M}$ corresponding only to a *local* minimum of Ω where M can be quite substantial. In other words, the 'lifetime' of a metastable thermodynamic state can be large compared with the time over which the microscopic evolution of the system can be pursued on account of limited computational speed. The origin of metastability is the lack of ergodicity in the immediate vicinity of a first-order phase transition which arises on account of the microscopically small systems employed in computer simulations [65]. Metastability is manifest as hysteresis in a sorption isotherm (like the one plotted in figure 8)—that is, a range of finite width Δs_z around the true transition point over which for the same T and μ, $\bar{\rho}(s_z)$ is a double-valued function. To distinguish the metastable from the thermodynamically (i.e. *globally*) stable phase one needs to compare Ω for the two states pertaining to different branches of the sorption isotherm at the same μ and s_z (see (17)). The one having lowest Ω is the globally stable phase; the other one is only metastable. In figure 8 we plot only data for thermodynamically stable phases identified according to this rationale.

4.2. The impact of shear strain

4.2.1. Lattice gas. The preceding section clearly illustrates the complex phase behaviour that one has to expect if fluids are confined between chemically decorated substrate surfaces.

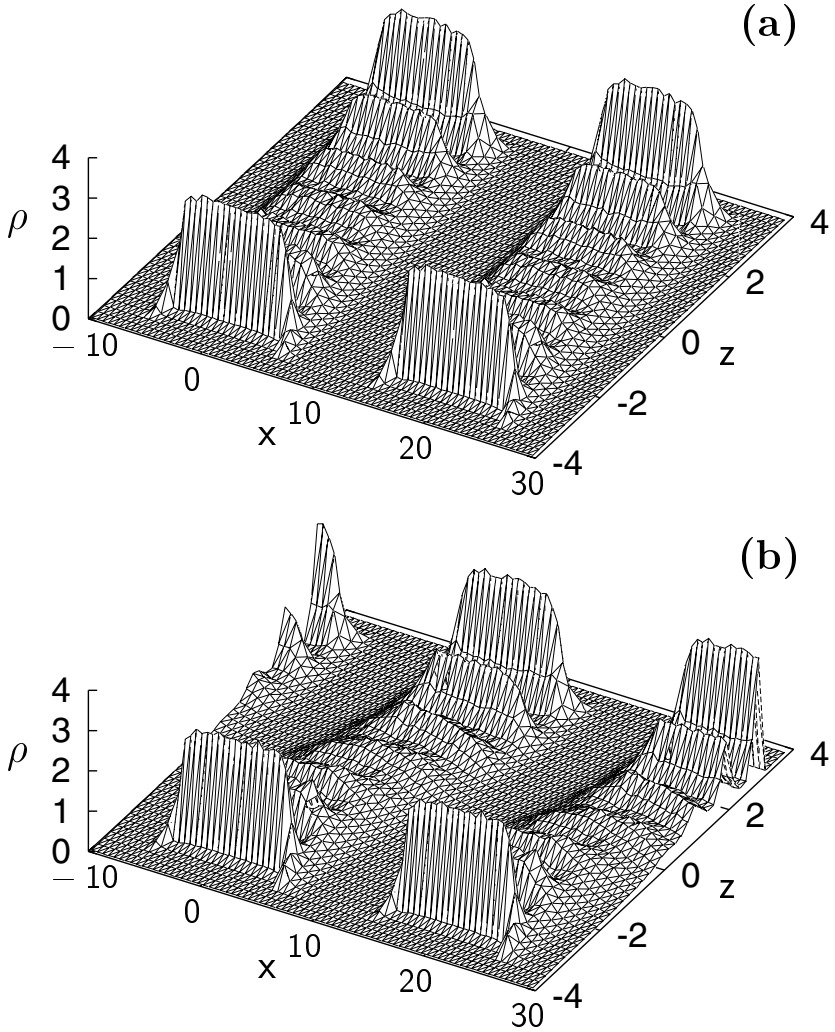

Figure 6. As figure 2, but for the continuous model. The plots show two periods of $\rho(x, z)$ in the x-direction because of the periodic boundary conditions: (a) unsheared bridge phase, $\alpha s_x = 0.0$; (b) sheared bridge phase, $\alpha s_x = 7.5$; (c) gaslike phase, $\alpha s_x = 10.0$; (d) liquidlike phase, $\alpha s_x = 10.0$. The plots in (c) and (d) correspond to coexisting phases. In all cases $T = 0.7$, $\mu = -8.15$, $s_x = 20.0$, $d_s = 10.0$, and $s_z = 8.0$.

This is particularly evident for the lattice gas where the relative simplicity of $\mathcal{F}$ permits one to calculate $\mu_x(T)$ which is determined by the three different length scales present in our model. In addition to the one set by the range of interactions between lattice-gas molecules (i.e., ℓ_{lg}), another one relates to confinement (i.e., n_z) and is already present if the substrates are chemically homogeneous. It causes:

(i) a critical-point shift to $\{\mu_c^{gl}, T_c^{gl}\}$ ($\epsilon_{fs} = \epsilon_{fw} > \epsilon_{ff}$) lower than the bulk $\{\mu_c, T_c\}$;
(ii) $\mu_x^{gl}(T)$ not to be parallel with the temperature axis.

The third length scale, introduced by chemical decoration of the substrate, is set by n_s (or, equivalently, $n_x - n_s$), exceeding ℓ_{lg} by almost an order of magnitude for the various coexistence

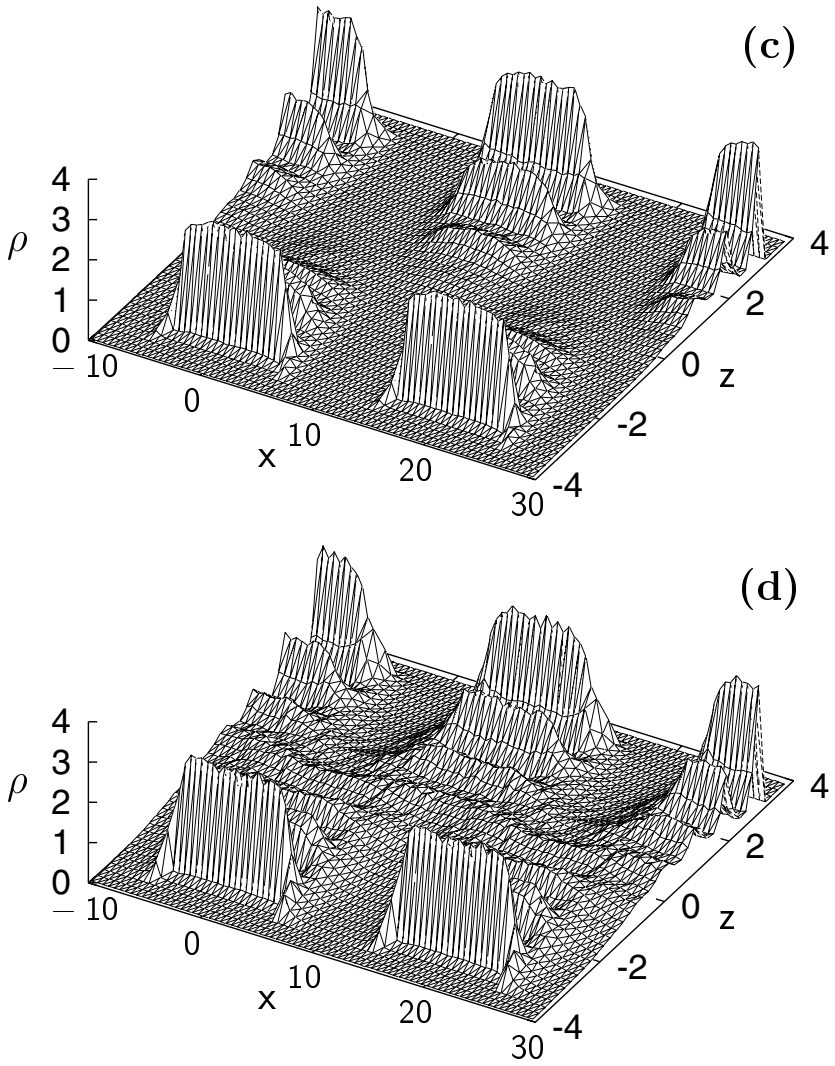

Figure 6. (Continued)

curves plotted in figure 4. The consequences of this third length scale are:

(i) existence of bridge phases as a new phase in the ordinary thermodynamic sense
(ii) two independent critical points $\{\mu_c^{gb}, T_c^{gb}\}$ and $\{\mu_c^{bl}, T_c^{bl}\}$.

Figure 4 already showed that the precise form of $\mu_x(T)$ is caused by an interplay of these different length scales.

To further elucidate this interplay it seems interesting to expose the lattice gas to a shear strain by varying α (see (5)). Comparing the plots in figure 2(a) and figure 2(b) illustrates the effect of a shear strain on the structure of a typical bridge phase. However, depending on the thermodynamic state a bridge phase will sustain only a maximum shear strain but will eventually be either 'torn apart' and undergo a first-order phase transition to a gaslike phase (see figure 2(c)) or condense and form a liquidlike phase (see figure 2(d)). The corresponding coexistence curves $\mu_x(T)$ plotted in figure 9 show that increasing α from its initial value

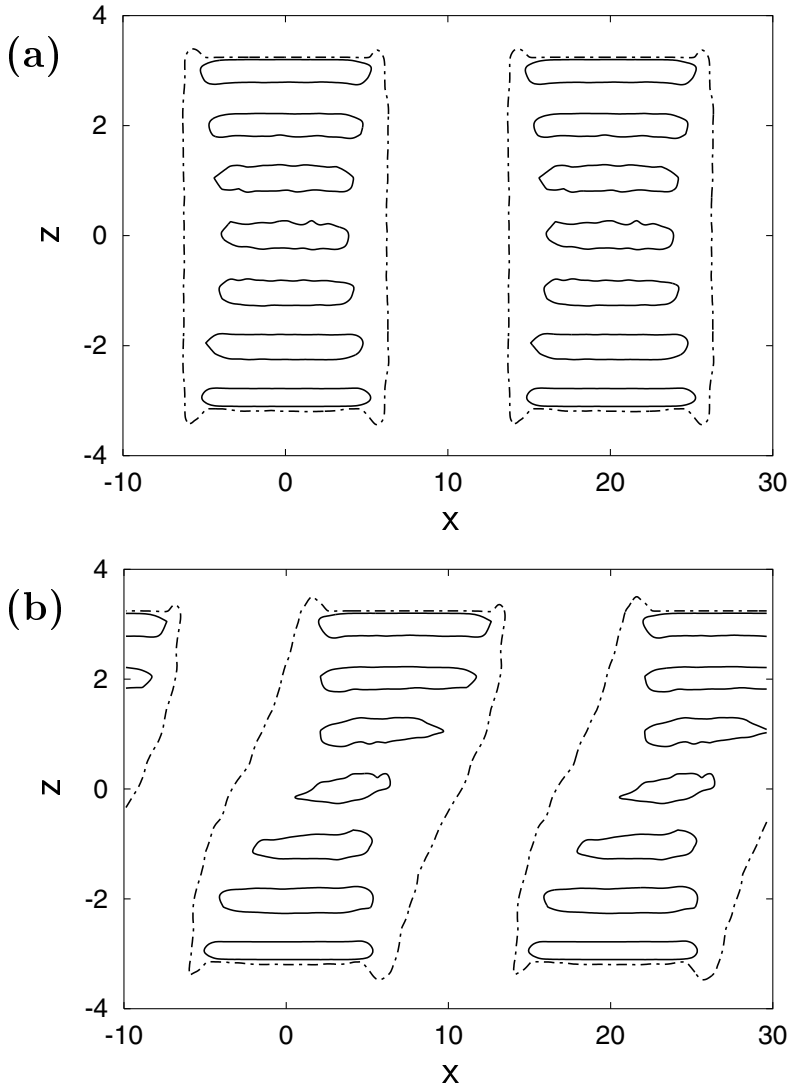

Figure 7. Contour lines $\rho(x, z) = 0.10$ (— · —), 0.75 (——) corresponding to the plots in figure 6.

of zero causes the triple point to shift to higher T_{tr} and μ_{tr}. Simultaneously, the one-phase region of the bridge phases shrinks. The one-phase regime of bridge phases may, however, vanish completely for some $\alpha < \alpha_{\max}$ depending on substrate separation (i.e., n_z), chemical corrugation (i.e., n_{s}/n_x), or strength of interaction with the chemically different parts of the substrate (i.e., ϵ_{fw}, ϵ_{fs}). Notice that for the special case $\alpha_{\max} = \frac{1}{2}$ (i.e., n_x even) the one-phase region of bridge phases *must* vanish in the limit $\alpha = \alpha_{\max}$ for symmetry reasons (see (4), (5)). In addition, figure 9 shows that critical temperatures $T_{\mathrm{c}}^{\mathrm{bl}}$ and $T_{\mathrm{c}}^{\mathrm{gb}}$ depend only weakly on the shear strain unlike $\mu_{\mathrm{c}}^{\mathrm{bl}}$ and $\mu_{\mathrm{c}}^{\mathrm{gb}}$, such that the critical points are essentially shifted upwards and downwards, respectively, as α increases.

Consider now a specific isotherm $T_x = 1.25$ in figure 9, intersecting with different branches of the (same) coexistence curve $\mu_{\mathrm{x}}(T)$ at different chemical potentials. According

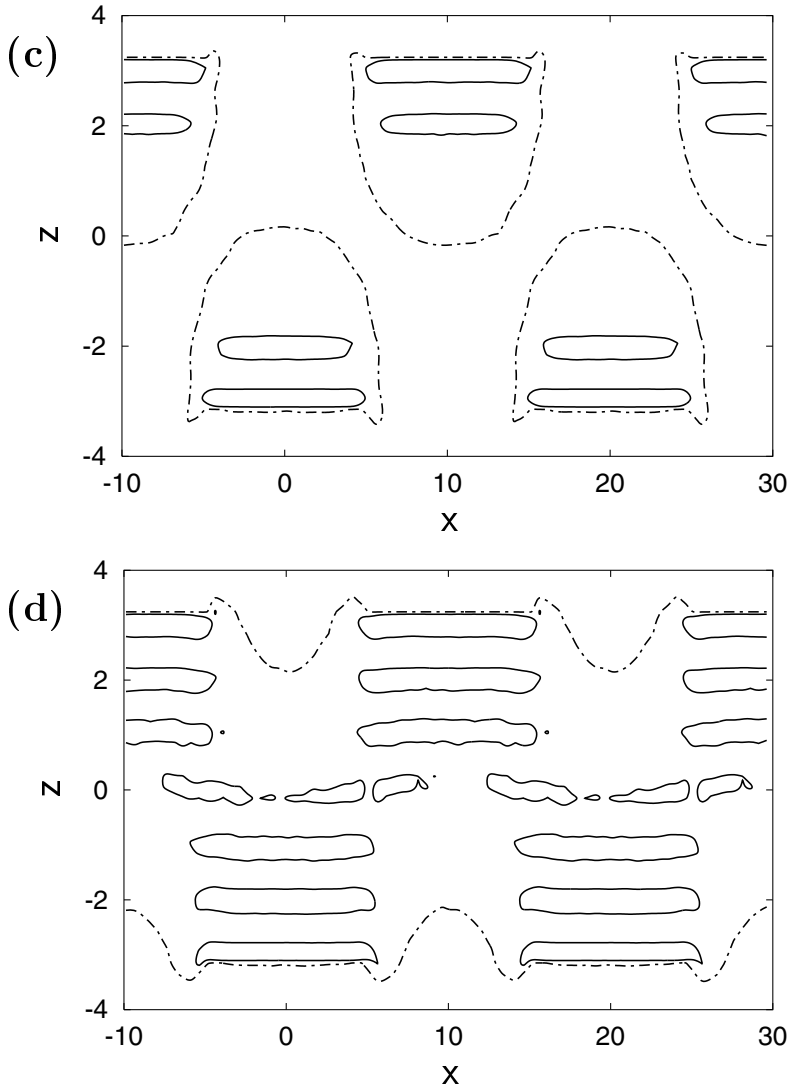

Figure 7. (Continued)

to the definition of $\mu_x(T)$, each intersection corresponds to a pair of (separately) coexisting phases. For example, at $\mu_x^{gb}(T_x) \simeq -3.053$ and $\alpha = 0$ a gaslike phase coexists with a (more dilute) bridge phase whereas a (denser) bridge phase coexists with a liquidlike phase for $\mu_x^{bl}(T_x) \simeq -3.029$. Because the one-phase region of bridge phases shrinks with α (see figure 9), the 'distance' $\Delta\mu_x(T_x) := |\mu_x^{gb}(T_x) - \mu_x^{bl}(T_x)| \to 0$ the larger α becomes, that is with increasing shear strain. From the plot in figure 9 it is clear that a shear strain exists such that $\Delta\mu_x = 0$, that is $T_x \leqslant T_{tr}(\alpha n_x)$. For this and larger shear strains, only a single intersection remains, corresponding to coexisting gaslike and liquidlike phases (see figure 9).

4.2.2. Continuous model. If the confined fluid in the continuous model is exposed to a shear strain, it undergoes structural transformations similar to the ones just discussed for the lattice

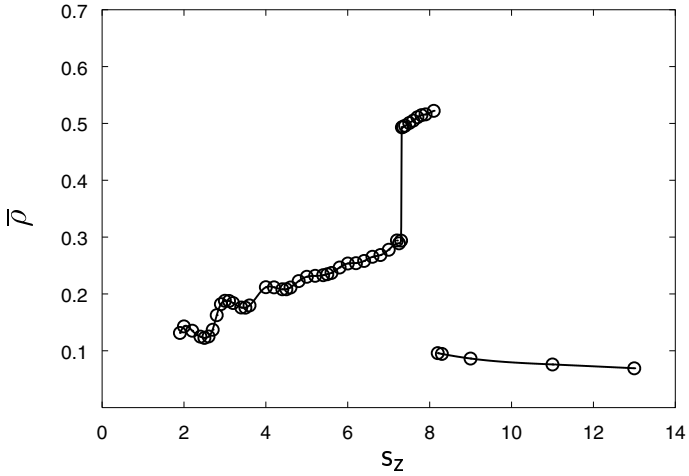

Figure 8. Average density $\bar{\rho}$ as a function of substrate separation s_z for the continuous model. Grand canonical ensemble Monte Carlo simulations were carried out for $T = 1.0$, $\mu = -11.5$, $s_x = 12.0$, $d_s = 4.0$, $\alpha s_x = 0.0$ (from [52]). Solid lines are intended to guide the eye.

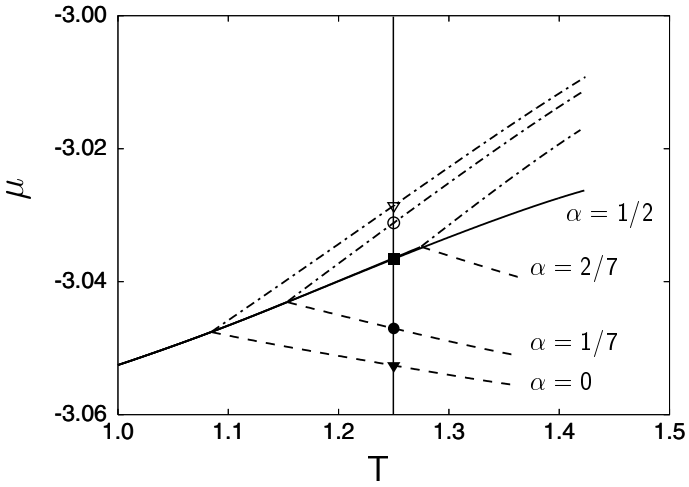

Figure 9. As figure 4(a), but for various shear strains α indicated in the figure ($n_x = 14$, $n_s = 6$, $n_z = 7$, $\epsilon_{fs} = 1.6$, $\epsilon_{fw} = 0.4$. Intersections between isotherm $\mathbb{T}$ (the vertical solid line; see the text) and the coexistence-curve branches represent coexisting phases: (▼) $\mu_x^{gb}(T_x)$, (▽) $\mu_x^{bl}(T_x)$, $\alpha = 0$; (●) $\mu_x^{gb}(T_x)$, (○) $\mu_x^{bl}(T_x)$, $\alpha = \frac{1}{7}$; (■) $\mu_x^{gl}(T_x)$, $\alpha = \frac{2}{7}$.

gas. For example, a bridge phase can sustain a shear strain (see figure 6(a), figure 6(b)). Comparing the corresponding contour plots in figure 7(a) and figure 7(b), one sees that as a result of the applied deformation, centres of molecular strata are displaced in the $+x$-direction. If the shear strain exceeds a certain threshold one expects from the lattice-gas results (see figure 9) the bridge phase to undergo a first-order phase transition. Depending on the 'position' of the thermodynamic state with respect to $\mu_x^{gb}(T)$ and $\mu_x^{bl}(T)$, either a gaslike or a liquidlike phase may form as a result. Both situations are realized, as plots in figure 6(c) and figure 6(d) reveal. Contour plots of $\rho(x, z)$ in figure 7(c) show that a typical gaslike phase consists of

isolated and stratified columns of fluid (because $\rho(x, z)$ is translationally invariant in the y-direction) stabilized by the strongly attractive parts of the substrate. For a liquidlike phase (see figure 7(d)) these columns are connected through a stratified portion of fluid centred on $z = 0$ (see figure 6(d)).

Because of the similarity between the lattice-gas calculations and the Monte Carlo simulations for the continuous model, it seems instructive to study the phase behaviour in the latter if the confined fluid is exposed to a shear strain. This may be done conveniently by calculating $\bar{\rho}$ as a function of μ and αs_x. Because of the microscopic size of the simulation cell, results are again affected by metastability in the immediate vicinity of a phase transition. To identify coexisting phases on the sorption isotherm we adopt the procedure described above in section 4.1.2.

For sufficiently low μ one expects a gaslike phase to exist along a subcritical isotherm $\mathbb{T} = \{(\mu, T)|\mu_{\rm tr} < \mu < \min(\mu_{\rm c}^{\rm gb}, \mu_{\rm c}^{\rm bl}), T_{\rm tr} < T < \min(T_{\rm c}^{\rm gb}, T_{\rm c}^{\rm bl}), T = \text{constant}\}$ (see figure 9). At an intersection between $\mathbb{T}$ and $\mu_{\rm x}^{\rm gb}(T)$, the gaslike phase will undergo a spontaneous transformation to a bridge phase. In a corresponding plot of $\bar{\rho}(\mu)$ one should see a discontinuous jump to a higher density. Eventually, another intersection between $\mathbb{T}$ and $\mu_{\rm x}^{\rm bl}(T)$ occurs and a second discontinuous jump to an even higher value of $\bar{\rho}(\mu)$ should be visible. Both of these transitions are indeed observed in figure 10 for $\alpha s_x = 0$, $\mu \simeq -8.40$, and $\mu \simeq -7.98$, respectively. Notice that in figure 10, $\mu_{\rm x}^{\rm bl}$ for $\alpha s_x = 0.0$ exceeds its bulk counterpart $\mu_{\rm x}^{\rm bulk}$; that is, for $\mu_{\rm x}^{\rm bl}$ the corresponding bulk phase is liquid. This can be rationalized by noting that the low(er)-density part of a bridge phase is predominantly involved in this second transition.

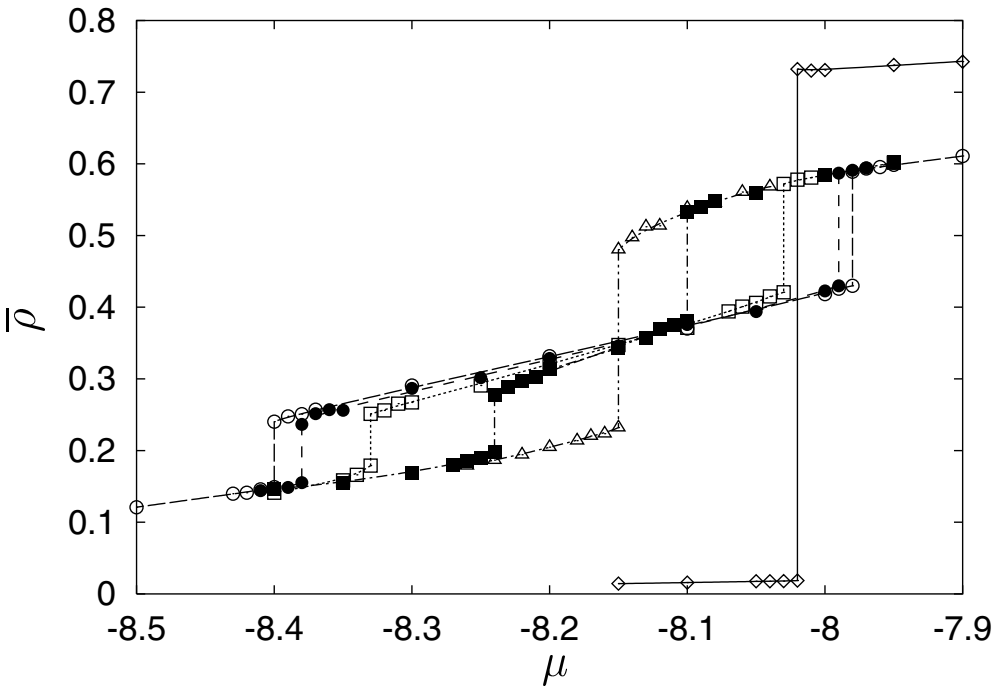

Figure 10. Sorption isotherms $\bar{\rho}(\mu)$ from grand canonical ensemble Monte Carlo simulations (continuous model); ○, – – –: $\alpha s_x = 0.0$; ●, - - - -: $\alpha s_x = 2.5$; □, ·····: $\alpha s_x = 5.0$; ■, — · —: $\alpha s_x = 7.5$; △, — · · —: $\alpha s_x = 10.0$. Also shown are corresponding bulk data (◇, ——). Results were obtained for $T = 0.7$, $s_x = 20.0$, $d_{\rm s} = 10.0$, and $s_z = 8.0$.

Recall also that this part of a bridge phase is stabilized by the *weak* portions of both (perfectly aligned) substrates characterized by $\epsilon_{\mathrm{fw}} \ll \epsilon_{\mathrm{ff}}$. Hence, the second first-order transition is inhibited rather than supported by the substrates (with respect to the bulk) because of the dominating repulsive interaction of a fluid molecule with the weak part of the substrate.

If a shear strain is applied, the region of overlap of the weak substrate parts in the x-direction shrinks (see (15)) such that a fluid molecule located at $\{x|d_{\mathrm{s}}/2 \leqslant |x| \leqslant s_x/2, \alpha s_x = 0.0\}$ is exposed to a stronger net attractive fluid–substrate interaction. Consequently, one expects an associated shift of $\mu_{\mathrm{x}}^{\mathrm{bl}}$ to lower values. The plot in figure 10 confirms the expectation. In addition, figure 9 shows that the one-phase region shrinks because T_{tr} shifts to higher temperatures and because the slope of the coexistence lines does not change much. The plot in figure 9 therefore suggests that for $\alpha > 0$ the two discontinuities in $\bar{\rho}(\mu)$ approach each other with the result that that the branch of $\bar{\rho}(\mu)$ pertaining to bridge phases becomes narrower with increasing αs_x. This effect is indeed visible in figure 10 where the width of the intermediate-density branch of $\bar{\rho}(\mu)$ (corresponding to thermodynamically stable bridge phases) diminishes from $|\Delta\mu| \simeq 0.42$ ($\alpha s_x = 0.0$) to $|\Delta\mu| \simeq 0.14$ ($\alpha s_x = 7.5$). Finally, if the shear strain is large enough, the lattice-gas results in figure 9 suggest that for a given temperature T^*, $T_{\mathrm{tr}}(\alpha s_x) > T^*$ for sufficiently large shear strains (see the curve for $\alpha = \frac{2}{7}$ in figure 9). Hence, under these circumstances one would expect $\bar{\rho}(\mu)$ to exhibit just a single discontinuity relating to a phase transition between gaslike and liquidlike phases. The plot in figure 10 for $\alpha s_x = 10$ confirms this prediction.

5. Discussion and conclusions

In this paper we discuss the phase behaviour of fluids confined to spaces of microscopic to mesoscopic dimensions by chemically corrugated solid substrates. The substrates consist of alternating portions of weakly and strongly adsorbing solid. We employ lattice-gas models at the mean-field level of description (see figure 1) and Monte Carlo simulations in the grand canonical ensemble (see figure 3) to investigate both the microscopic structure of the confined ('simple') fluid and its relation to the overall phase behaviour. Since the substrates themselves are chemically patterned, they offer the possibility of exposing the confined fluid to a shear strain. Therefore, the key issue of this work is the impact of shear strain on first-order phase transitions in the confined fluid. Our results can be summarized as follows:

(i) Depending on the thermodynamic state, a fluid confined between chemically decorated substrates may form a gaslike, liquidlike, or bridge phase (see figure 2, figure 6, figure 7).

(ii) A triple point $\{\mu_{\mathrm{tr}}, T_{\mathrm{tr}}\}$ exists at which all three phases coexist. For $T < T_{\mathrm{tr}}$, gaslike and liquidlike phases are in thermodynamic equilibrium with each other along the coexistence curve $\mu_{\mathrm{x}}^{\mathrm{gl}}(T)$. For $T > T_{\mathrm{tr}}$, a gaslike phase coexists with a bridge phase along $\mu_{\mathrm{x}}^{\mathrm{gb}}(T)$ whereas a bridge phase coexists with a liquidlike phase independently along $\mu_{\mathrm{x}}^{\mathrm{bl}}(T)$. Both coexistence curves terminate at their respective critical points $\{\mu_{\mathrm{c}}^{\mathrm{gb}}, T_{\mathrm{c}}^{\mathrm{gb}}\}$ and $\{\mu_{\mathrm{c}}^{\mathrm{bl}}, T_{\mathrm{c}}^{\mathrm{bl}}\}$ (see figure 4(a)).

(iii) In the absence of a shear strain (i.e., for $\alpha = 0$):

  (a) From the lattice-gas calculations one expects two first-order phase transitions if μ is varied along an isotherm $\mathbb{T}$. The one at lower μ involves a gaslike and a bridge phase whereas a transition from a bridge to a liquidlike phase is expected at higher μ (see figure 9). In the continuous model these transitions are manifest as discontinuities in $\bar{\rho}$ separated by a 'distance' $\Delta\mu$ (see figure 10).

  (b) Lattice-gas calculations reveal that gas–liquid (i.e., $\mu_{\mathrm{x}}^{\mathrm{gl}}(T)$), gas–bridge (i.e., $\mu_{\mathrm{x}}^{\mathrm{gb}}(T)$), and bridge–liquid (i.e., $\mu_{\mathrm{x}}^{\mathrm{bl}}(T)$) branches of the coexistence curve as well as the

triple-point location $\{\mu_{tr}, T_{tr}\}$ depend on the substrate separation in a complex manner (see figure 4(a)). Thus, if the thermodynamic state is chosen suitably, one expects two first-order phase transitions upon reducing s_z at constant T and μ. The one at larger s_z relates to condensation of a gaslike to a liquidlike phase which, in turn, undergoes a subsequent transition to a bridge phase at smaller s_z (see figure 4(b)) in accord with Monte Carlo results for the continuous model (see figure 8).

(iv) With exposure to shear strain (i.e., for $\alpha \neq 0$):

(a) In the lattice-gas model T_{tr} increases with α. Simultaneously, $\mu_x^{gb}(T)$ and $\mu_x^{bl}(T)$ become shorter such that the one-phase region of bridge phases shrinks (see figure 9). This effect is also detected in Monte Carlo simulations of the continuous model where the 'distance' $\Delta\mu$ between the discontinuities in $\bar{\rho}$ diminishes ($T > T_{tr}(\alpha s_x)$; see figure 10).

(b) If for a given temperature T^* the shear-strain-induced shift of $T_{tr}(\alpha s_x)$ is such that $T^* < T_{tr}(\alpha s_x)$, the lattice-gas calculations suggest a single first-order transition involving only gaslike and liquidlike phases (see figure 9). Again this notion is confirmed by the parallel Monte Carlo data (see figure 10).

(c) A point $\Gamma = \{(\mu, T)|\mu_x^{gb}(T) < \mu < \mu_x^{bl}(T), T_{tr} < T < \min(T_c^{gb}, T_c^{bl})\}$ representing a thermodynamic state in the one-phase region of bridge phases may be located relative to the coexistence lines $\mu_x^{gb}(T)$ and $\mu_x^{bl}(T)$ for $\alpha = 0$ such that upon increasing α the bridge phase may undergo a first-order phase transition and form either a gaslike or a liquidlike phase (see figure 2, figure 6, figure 7).

The qualitative similarity between the phase behaviour of fluids in the present, rather regular model and that reported for disordered porous media [60] may suggest that phenomena observed here could also be present in experimental systems. For example, if a fluid condenses only in certain parts of a mesoporous medium on account of its structural or chemical heterogeneity, one would expect sorption isotherms exhibiting several discontinuous 'steps' similar to the ones in figure 10. Upon decreasing T, the locations of these discontinuities should approach each other, with only a single one remaining for sufficiently low T. Alternatively, one may measure calorimetrically the latent heat associated with the various first-order phase transitions. This should be feasible because our lattice-gas results in figure 5 show that, compared with those for the bulk, the molar enthalpies of vaporization of confined phases are not drastically smaller.

The mean-field lattice gas is a convenient simple, yet not entirely unrealistic statistical-physical model of a fluid (i.e., gas or liquid). Because of its apparent simplicity it is relatively easy to construct entire phase diagrams numerically even if the present anisotropic and local lattice-gas model is involved. In Monte Carlo simulations, on the other hand, one obtains results for a given model of (*in principle*) arbitrary complexity essentially in a first-principles fashion. The disadvantage is that, compared with the case for the mean-field lattice gas, a determination of phase diagrams for more realistic models in these simulations is computationally much more demanding. We notice that powerful Monte Carlo methods like the histogram-reweighting technique [66] exist by which first-order phase transitions can be studied efficiently. However, it seems worthwhile emphasizing that the focal point of this study is not calculating complete phase diagrams by Monte Carlo methods. Rather, we are interested in finding out to what extent the simplistic mean-field lattice gas provides a realistic model of fluids confined between chemically decorated substrate surfaces, since we plan to extend the present study to confined binary mixtures in the near future. In the latter context the lattice gas should be useful to assist the interpretation of parallel computer simulations where the exploration of the vast

parameter space is inevitably limited. In the light of this study a combination of simulations and lattice-gas calculations at mean-field level is expected to be highly profitable.

Acknowledgments

We thank Professor R Evans (University of Bristol) for helpful discussions and insightful comments concerning the formal treatment of the mean-field lattice gas from which the appendix of this paper emerged. We are grateful to the Sonderforschungsbereich 448 'Mesoskopisch strukturierte Verbundsysteme' for financial support. Two anonymous referees are acknowledged for helpful comments as is the Konrad-Zuse-Zentrum für Informationstechnik for a generous allotment of computer time.

Appendix A. Grand potential functional for an inhomogeneous mean-field lattice gas

Here we present a derivation of (2) and (3) appearing in section 2.1. Consider N classical spins $\sigma(\boldsymbol{r}) = \pm 1$ on a three-dimensional lattice where the vector $\boldsymbol{r}$ specifies a particular site. The pairwise-additive interaction between spins and between a spin and an external magnetic field is described by an Ising (-type) model where the Hamiltonian is given by

$$H_{\mathrm{I}} = -\sum_{\boldsymbol{r}} \sigma(\boldsymbol{r}) \left[J \sum_{\boldsymbol{r}'}{}' \sigma(\boldsymbol{r}') + H(\boldsymbol{r}) \right] =: -\sum_{\boldsymbol{r}} H_{\mathrm{eff}}(\boldsymbol{r}; \{\sigma(\boldsymbol{r}')\})\sigma(\boldsymbol{r}). \tag{A.1}$$

In (A.1), coupling constant J determines the strength of interaction between a pair of spins, and the prime attached to the summation sign signals that only nearest-neighbour spins interact. We deviate from the classical Ising model by incorporating a local (rather than a constant) magnetic field $H(\boldsymbol{r})$. The term in brackets may thus be interpreted as an *effective* local magnetic field H_{eff} exerted on $\sigma(\boldsymbol{r})$ due to $H(\boldsymbol{r})$ and the neighbouring spins. Therefore, $H_{\mathrm{eff}}(\boldsymbol{r}; \{\sigma(\boldsymbol{r}')\})$ depends on the *actual* configuration $\{\sigma(\boldsymbol{r}')\}$ of nearest-neighbour spins.

To simplify (A.1) we adopt a mean-field approximation assuming that

$$\begin{aligned} &\sigma(\boldsymbol{r}') \to \langle \sigma(\boldsymbol{r}') \rangle \equiv m(\boldsymbol{r}') \\ &H_{\mathrm{eff}}(\boldsymbol{r}; \{\sigma(\boldsymbol{r}')\}) \to \widetilde{H}_{\mathrm{eff}}(\boldsymbol{r}; \{m(\boldsymbol{r}')\}) \end{aligned} \tag{A.2}$$

where the locally constant magnetization $m(\boldsymbol{r}')$ in thermodynamic equilibrium is a continuous function on the interval $[-1, +1]$ and the effective local magnetic field in the mean-field approximation, $\widetilde{H}_{\mathrm{eff}}(\boldsymbol{r}; \{m(\boldsymbol{r}')\})$, is independent of $\{\sigma(\boldsymbol{r}')\}$ but depends on the set of (locally constant) magnetizations at neighbouring lattice sites. Henceforth we shall therefore drop $\{m(\boldsymbol{r}')\}$ as an implicit argument of $\widetilde{H}_{\mathrm{eff}}$ to simplify the notation. Thus, at the mean-field level $H_{\mathrm{I}} = \sum_{\boldsymbol{r}} h(\boldsymbol{r})$ where the single-spin Hamiltonian is given by

$$h(\boldsymbol{r}) = -\widetilde{H}_{\mathrm{eff}}(\boldsymbol{r})\sigma(\boldsymbol{r}). \tag{A.3}$$

Based upon (A.2), a molecular expression for $m(\boldsymbol{r})$ is obtained from the statistical-physical expression (canonical ensemble):

$$\begin{aligned} m(\boldsymbol{r}) &= \left(\sum_{\sigma(\boldsymbol{r})} \sigma(\boldsymbol{r}) \exp[-h(\boldsymbol{r})/k_{\mathrm{B}}T] \right) \Big/ \left(\sum_{\sigma(\boldsymbol{r})} \exp[-h(\boldsymbol{r})/k_{\mathrm{B}}T] \right) \\ &= \tanh[\widetilde{H}_{\mathrm{eff}}(\boldsymbol{r})/k_{\mathrm{B}}T] = \tanh\left\{ \frac{1}{k_{\mathrm{B}}T} \left[H(\boldsymbol{r}) + J \sum_{\boldsymbol{r}'}{}' m(\boldsymbol{r}') \right] \right\}. \end{aligned} \tag{A.4}$$

Equation (A.4) can be rewritten in lattice-gas rather than magnetic language, employing the following identifications [55]:

$$\begin{aligned} J &= \frac{\epsilon_{\mathrm{ff}}}{4} \\ H(\boldsymbol{r}) &= \frac{1}{2}\left[\mu - \frac{\epsilon_{\mathrm{ff}}}{2} - \Phi(\boldsymbol{r})\right] \\ m(\boldsymbol{r}) &= 2\rho(\boldsymbol{r}) - 1 \end{aligned} \tag{A.5}$$

where the local density is defined on the interval [0, +1]. Equations (A.4) and (A.5) give

$$k_{\mathrm{B}}T \ln \frac{\rho(\boldsymbol{r})}{1-\rho(\boldsymbol{r})} - \mu + \Phi(\boldsymbol{r}) - \epsilon_{\mathrm{ff}} {\sum_{\boldsymbol{r}'}}' \rho(\boldsymbol{r}') = 0 \tag{A.6}$$

which may be perceived as the Euler–Lagrange equation resulting from (1). Thus, (2) and (3) are obtained directly by integrating (A.6) formally where, of course, $\Omega[0] = 0$ is also used. Equation (A.6) was presented earlier by Bruno *et al* [67], Röcken and Tarazona [49], and us [52] with (2) and (3) as starting points without further justification.

Evans has pointed out that an alternative way of deriving an expression for $\mathcal{S}$ in (3) is that of considering an ensemble of N noninteracting spins ($J = 0$) subjected to $H(\boldsymbol{r})$ [68]. In this case $h(\boldsymbol{r}) \equiv H(\boldsymbol{r})$ and we obtain (A.6) for $\epsilon_{\mathrm{ff}} = 0$ which is now exact. Formal integration of this latter expression yields $\mathcal{S}$ in (3) (when summed over $\boldsymbol{r}$). Together with a mean-field treatment of the spin–spin interaction (leading to a mean-field $\mathcal{U}$), $\mathcal{F}$ as presented in (3) is eventually obtained.

References

[1] Bönsch P, Wüllner D, Schrimpf T, Schlachletzki A and Lacmann R 1998 *J. Electrochem. Soc.* **145** 1273
[2] Tolfree D W L 1998 *Rep. Prog. Phys.* **61** 313
[3] Xia Y and Whitesides G M 1998 *Annu. Rev. Mater. Sci.* **28** 153
[4] Burmeister F, Schläfle C, Keilhofer B, Bechinger C, Boneberg J and Leiderer P 1998 *Adv. Mater.* **10** 495
[5] Rogers J A, Bao Z and Dhar L 1998 *Appl. Phys. Lett.* **73** 294
[6] Aizenberg J, Black A J and Whitesides G M 1998 *Nature* **394** 868
[7] Kumar A and Whitesides G M 1993 *Appl. Phys. Lett.* **63** 2002
[8] Drelich J, Miller J D, Kumar A and Whitesides G M 1994 *Colloids Surf.* A **93** 1
[9] Wilbur J L, Kumar A, Kim E and Whitesides G M 1994 *Adv. Mater.* **6** 600
[10] Knight J B, Vishwanath A, Brody J P and Austin R H 1998 *Phys. Rev. Lett.* **80** 3863
[11] Grunze M 1999 *Science* **283** 41
[12] Casagrande C, Fabre P, Raphaël E and Veyssié M 1989 *Europhys. Lett.* **9** 251
[13] de Gennes P G 1991 *Rev. Mod. Phys.* **64** 645
[14] Borówko M and Patrykiejew A 2000 *Computational Methods in Colloid and Interface Science* ed M Borówko (New York: Dekker) at press
[15] Gelb L D, Gubbins K E, Radhakrishnan R and Sliwinska-Bartkowiak M 1999 *Rep. Prog. Phys.* **62** 1573
[16] Dietrich S 1988 *Phase Transitions and Critical Phenomena* vol 12, ed C Domb and J L Lebowitz (London: Academic) p 1
[17] de Gennes P G 1985 *Rev. Mod. Phys.* **57** 827
[18] Schick M 1990 *Liquides aux Interfaces (Les Houches 1988 Session XLVIII)* ed J Charvolin, J F Joanny and J Zinn-Justin (Amsterdam: Elsevier) p 415
[19] Sullivan D E and Telo da Gama M M 1986 *Fluid Interfacial Phenomena* ed C A Croxton (New York: Wiley) p 45
[20] Evans R 1992 *Fundamentals of Inhomogeneous Fluids* ed D Henderson (New York: Dekker) p 85
[21] Bauer C and Dietrich S 1999 *Phys. Rev.* E **60** 6919
[22] Cole M W and Vittoratos E 1976 *J. Low Temp. Phys.* **22** 223
[23] Chmiel C, Karykowski K, Patrykiejew A, Rzysko W and Sokolowski S 1994 *Mol. Phys.* **81** 691
[24] Röcken P, Somoza A, Tarazona P and Findenegg G H 1998 *J. Chem. Phys.* **108** 8689
[25] Douglas Frink L J and Salinger A G 1999 *J. Chem. Phys.* **110** 5969

[26] Nath S K, Nealey P F and de Pablo J J 1999 *J. Chem. Phys.* **110** 7483
[27] Gau H, Herminghaus S, Lenz P and Lipowsky R 1999 *Science* **283** 46
[28] Pomeau Y and Vannimenus J 1985 *J. Colloid Interface Sci.* **104** 477
[29] Robbins M O, Andelman D and Joanny J-F 1991 *Phys. Rev.* A **43** 4344
[30] Boulter C J 1998 *Phys. Rev.* E **57** 2062
[31] Lenz P and Lipowsky R 1998 *Phys. Rev. Lett.* **80** 1920
[32] Swain P S and Lipowsky R 1998 *Langmuir* **14** 6772
[33] Swain P S and Lipowsky R 2000 *Europhys. Lett.* **49** 203
[34] Lipowsky R, Lenz P and Swain P S 1999 *Colloids Surf.* A **161** 3
[35] Thommes M and Findenegg G H 1994 *Langmuir* **10** 4270
[36] Burgess G V, Everett D H and Nutall S 1989 *Pure Appl. Chem.* **61** 1845
[37] de Keizer A, Michalski T and Findenegg G H 1991 *Pure Appl. Chem.* **63** 1495
[38] Machin W D 1994 *Langmuir* **10** 1235
[39] Wong A P Y, Kim S B, Goldburg W I and Chan M H W 1993 *Phys. Rev. Lett.* **70** 954
[40] Wong A P Y and Chan M H W 1990 *Phys. Rev. Lett.* **65** 2567
[41] Evans R 1990 *Liquides aux Interfaces (Les Houches 1988 Session XLVIII)* ed J Charvolin, J-F Joanny and J Zinn-Justin (Amsterdam: North-Holland)
[42] Schoen M and Diestler D J 1998 *J. Chem. Phys.* **109** 5596
[43] Evans R 1990 *J. Phys.: Condens. Matter* **2** 8989
[44] Nakanishi H and Fisher M E 1983 *J. Chem. Phys.* **78** 3279
[45] Fisher M E and Nakanishi H 1981 *J. Chem. Phys.* **75** 5857
[46] Evans R, Marini Bettolo Marconi U and Tarazona P 1986 *J. Chem. Soc. Faraday Trans.* II **82** 1763
[47] Tarazona P, Marini Bettolo Marconi U and Evans R 1987 *Mol. Phys.* **60** 573
[48] Tovbin Y K and Votyakov E V 1993 *Langmuir* **9** 2652
[49] Röcken P and Tarazona P 1996 *J. Chem. Phys.* **105** 2034
[50] Schoen M and Diestler D J 1997 *Chem. Phys. Lett.* **270** 339
[51] Schoen M and Diestler D J 1997 *Phys. Rev.* E **56** 4427
[52] Bock H and Schoen M 1999 *Phys. Rev.* E **59** 4122
[53] Bock H and Schoen M 2000 *J. Phys.: Condens. Matter* **12** 1545
[54] Schoen M and Bock H 2000 *J. Phys.: Condens. Matter* **12** A333
[55] Baxter R J 1991 *Exactly Solved Models in Statistical Physics* (London: Academic)
[56] Stanley H E 1971 *Introduction to Phase Transitions and Critical Phenomena* (London: Academic) ch 6.3
[57] Törnig W 1979 *Numerische Mathematik für Physiker und Ingenieure* vol 1 (Berlin: Springer) p 259
[58] Allen M P and Tildesley D J 1987 *Computer Simulation of Liquids* (Oxford: Clarendon)
[59] Schoen M 2000 *Computational Methods in Colloid and Interface Science* ed M Borówko (New York: Dekker)
[60] Kierlik E, Rosinberg M L, Tarjus G and Monson P A 1998 *Fundamentals of Adsorption* ed F Meunier (New York: Elsevier) p 867
[61] Adams D J 1974 *Mol. Phys.* **28** 1241
[62] Schoen M 1999 *Physica* A **270** 353
[63] Schoen M, Diestler D J and Cushman J H 1987 *J. Chem. Phys.* **87** 5464
[64] Wilding N B and Schoen M 1999 *Phys. Rev.* E **60** 1081
[65] Schoen M, Rhykerd C L Jr, Diestler D J and Cushman J H 1989 *Mol. Phys.* **66** 1171
[66] Swendsen R H 1993 *Physica* A **194** 53
[67] Bruno E, Marini Bettolo Marconi U and Evans R 1987 *Physica* A **141** 187
[68] Evans R 1999 private communication with M Schoen